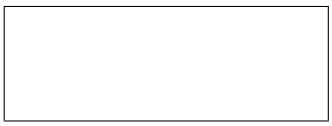

Characteristics and Environmental Conditions of Quasi-Stationary Convective Clusters during the Warm Season in Japan

Takashi Unuma* and Tetsuya Takemi

Disaster Prevention Research Institute, Kyoto University, Japan

*Correspondence to: Takashi Unuma, Gokasho, Uji, Kyoto 611-0011, Japan. E-mail: unuma_t@storm.dpri.kyoto-u.ac.jp

The characteristics and environmental properties of warm-season quasi-stationary convective clusters (QSCCs) in Japan were statistically investigated using operational weather radar and upper-air sounding data from May to October during 2005–2012. The characteristics of the environmental conditions for the development of QSCCs were described through a comparison with those for no-rain cases. We identified 4,133 QSCCs over the Japanese major islands. By compiling numerous QSCC samples, the horizontal scales of QSCCs on average and at the maximum with a circular shape are about 20 km and 72 km, respectively, indicating that warm-season QSCCs in Japan are meso-β-scale phenomena. The analyses of the environmental conditions for the QSCC and no-rain cases showed that the amount of moisture in the lower layer controls the stability condition for the development of the QSCCs, and that the magnitudes of the wind shear and the helicity in the lower troposphere distinguish the kinematic environments for the development of the QSCCs. An increase in the middle-level moisture leads to a larger amount of precipitable water vapor in the QSCC environments, suggesting that atmospheric moistening before the development stage of convection plays an important role in the development of the QSCCs. Additionally, the precipitation intensity has a higher correlation with the convective instability, whereas the precipitation area with the shear intensity. A comparison between slower- and the faster-moving CCs indicated that the precipitation intensity of the slower-moving CCs is stronger. This feature is related to a higher convective instability for the slower-moving ones.

Key Words: quasi-stationary convective cluster, moisture contribution, stability, radar-analysis

Received . . .

Citation: . . .

1. Introduction

[0]Please ensure that you use the most up to date class file, available from the QJRMS Home Page at
http://onlinelibrary.wiley.com/journal/10.1002/(ISSN)1477-870X

Understanding and predicting warm-season convective rainfall remain challenging tasks from both research and operational perspectives. Warm-season convective rainfall can sometimes be a significant event that spawns water-related disasters. Simply stated, heavier rainfall occurs where a high rainfall rate continues for an extended time (Chappell 1986; Doswell *et al.* 1996). As a cause of disaster-spawning heavy rain events, mesoscale convective systems (MCSs) act as key players among weather phenomena during the warm season. MCSs are defined as a cloud system that produces a contiguous precipitation area on the order of 100 km or more on a horizontal scale in at least one direction (Glickman 2000).

MCSs are widespread phenomena that develop in various climate regions ranging from tropical, sub-tropical, to extra-tropical regions. It is anticipated that locations with a stronger rainfall rate over an extended period will produce a heavier rainfall in the presence of a longer-lived MCS. From the Eulerian perspective, heavier rainfall is caused by the presence of a longer-lived and stationary (or slow-moving) MCS.

MCSs appear to be quasi-stationary due to two factors: 1) convective cells are continuously generated in similar locations by a back-building process (Bluestein and Jain 1985) under a stationary or slowly changing synoptic-weather condition (such as a stationary front), and 2) convective cells are continuously generated by topographic forcing. For example, Schumacher and Johnson (2008) examined an extreme rain event in the United States that occurred under quasi-stationary, synoptic-scale weather conditions where convective cells were successively generated by quasi-stationary forcings. On the other hand, complex topography plays a role in triggering and enhancing flash-flood-producing events over the Alpine region (e.g., Buzzi and Foschini 2000; Anquetin *et al.* 2003; Davolio *et al.* 2009; Panziera *et al.* 2014). In addition,

quasi-stationary convective systems found in the southern part of the United Kingdom develop due to forcing from sea breezes (Warren *et al.* 2014).

[Figure 1 about here.]

Quasi-stationary convective systems are a well-known cause of heavy rainfall in Japan. Such events frequently appear during the warm season (Ogura 1991; Yoshizaki and Kato 2007) under the presence of extra-tropical cyclones, synoptic-scale fronts, tropical cyclones, or stationary fronts such as Baiu fronts. The horizontal scale of a precipitating system over Japan is typically on the order of 10 km, which corresponds to the meso-β-scale by the definition of Orlanski (1975).

The environmental conditions necessary to develop quasi-stationary convective systems, particularly during the Baiu season, are characterized by a larger moisture content (Kato 2006; Hirockawa and Kato 2012). Higher environmental moisture may be a common feature for MCS events over East Asia; for example, Meng *et al.* (2013) showed that precipitable water is higher for the MCSs in east China than for those in the United States. In addition to such humid conditions, kinematic effects such as low-level convergences and vertical shears of horizontal winds play important roles in maintaining quasi-stationary convective systems (Kato 1998; Kato and Goda 2001; Kato and Aranami 2005; Yoshizaki *et al.* 2000). Kato (2005) examined the conditions favorable for the development of quasi-stationary convective systems over Kyushu Island, which is located in the western part of Japan, and found that the presence of persistent southwesterly winds is required to form quasi-stationary convective systems. In addition, Yoshizaki *et al.* (2000) showed that topographic forcing is important to

trigger convective clouds and organize quasi-stationary convective systems over the western part of Kyushu Island. In this way, many studies have investigated quasi-stationary convective systems with significant societal impacts and/or have employed special campaigns as a case-study basis.

However, few have investigated the statistical or climatological features of quasi-stationary convective systems in Japan by compiling numerous samples. One exception was conducted by Chuda and Niino (2005); through an investigation of the features of the background atmospheric conditions over Japan in terms of environmental parameters using radiosonde data, they showed that the environmental parameters strongly depend on the location and the season. Convective available potential energy (CAPE) values generally become larger at lower latitudes and during the warmer season; thus, convective storms favor to develop in the southern parts of Japan during the warmer season. Because their study did not distinguish the environmental conditions for convective events from non-convective events, the environmental characteristics for the development of quasi-stationary convective systems in Japan remain unknown.

The distinction between convective and non-convective environments should help our understanding on the general conditions necessary to develop convective precipitation. A statistical analysis for afternoon thunderstorms over the Kanto area (see Figure 1(b)) in the summer was conducted by (Nomura and Takemi 2011). Nomura and Takemi examined 11 environmental parameters for afternoon rain cases by comparing with no-rain cases with the use of mesoscale-gridded analysis data by Japan Meteorological Agency (JMA) as well as the radiosonde data observed at Tateno (see Figure 1(b)). The K Index significantly distinguishes

the environmental conditions between the rain and the no-rain cases. They also investigated the vertical structures of temperature and moisture, and concluded that colder temperatures at middle levels and higher humidity at low to middle levels are the conditions favorable for afternoon rains.

A similar analysis was conducted for afternoon rain events in and around the Nobi Plain located in central Japan (Takemi 2014a). In addition, Kato (2006)'s case studies suggested that the middle-level moisture plays an important role in determining the development of convective systems. However, statistical studies that specifically focus on quasi-stationary convective systems have yet to be conducted. In this study, which focuses on various types of convective systems, including a cluster of convective clouds, we refer to quasi-stationary convective systems as quasi-stationary convective clusters (QSCCs).

The purpose of this study is to reveal the climatological features of QSCCs, including lifetime, location, rain intensity, and the environmental properties for the development of QSCCs during the warm season over Japan. The analyses were performed using operational radar and upper-air observation data. To identify QSCCs, we modified a method to detect an individual convection cell within a precipitating area from radar observations (Shimizu and Uyeda 2012). The environmental characteristics for the development of QSCCs were examined in terms of the environmental parameters by comparing QSCC events and no-rain cases using idea similar to Nomura and Takemi (2011) and Takemi (2014a). From the environmental analyses, we revealed the conditions favorable for the development of QSCCs from a climatological point of view. Because Barnes and Sieckman (1984) showed that there are similarities and differences of the environments for fast- and slow-moving

mesoscale convective cloud lines over the tropics, we also examined the differences of the characteristics and environmental properties of QSCCs by dividing them into sub-groups based on their propagation speed (i.e., slower-moving CCs and faster-moving CCs). Through a demonstration of the specific parameters used to diagnose the development of QSCCs, it is emphasized here that statistical information can be used as a better forecasting guide for the development of QSCCs.

2. Data and methodology

2.1. Data

The data observed during the warm season, i.e., from May to Octorber, during 2005–2012 are used in this study. To identify QSCCs, we use operational radar data of JMA. In this dataset, the radar reflectivities from 19 elevation angles within the detection range of 200 km are converted to precipitation intensities at the height of about 2 km. This study uses this precipitation intensity dataset. The unit of the data is mm h^{-1}. The horizontal resolutions on the longitude-latitude grid is approximately 1 km (hereafter referred to as 1 km), and the temporal interval is 10 minutes, which are sufficiently high for identifying and tracking QSCCs all over Japan. Since the present study deals with QSCCs that develop over land, the area for the analysis of the radar precipitation intensity is limited to the Japanese major islands and the surrounding region within 10 km off the coast. The locations and ranges of those radars are shown in Figure 1(a).

The upper-air sounding data by radiosondes are used to examine the environmental conditions for the development of the extracted QSCCs. Figure 1(b) shows the locations

of these stations: Wakkanai (WKN), Sapporo (SPR), Kushiro (KSR), Nemuro (NMR), Akita (AKT), Wajima (WJM), Tateno (TTN), Hamamatsu (HMT), Matsue (MTE), Yonago (YNG), Shionomisaki (SNM), Fukuoka (FKO), and Kagoshima (KGS). Note that the Nemuro (Yonago) station was re-located to Kushiro (Matsue) in March 2010, and thus the Nemuro (Yonago) station is regarded as the same with the Kushiro (Matsue) station. We consider that the differences that may arise owing to this re-location are minimal in the analysis on the environmental conditions because the re-located stations belong to similar climate regions. The times of the upper-air observations are 0900 and 2100 Japan Standard Time (JST), which is 9 hours plus UTC. Hereafter the times are referred to as JST.

2.2. *Identification and tracking of QSCCs*

To extract QSCCs, we use Algorithm for the Identification and Tracking Convective Cells (AITCC) that was developed by Shimizu and Uyeda (2012). This algorithm was originally intended to identify and track individual convective cells within an MCS. We modify the algorithm for identifying and tracking QSCCs. The procedures of how to extract QSCCs are described here.

The first procedure is to extract convective clusters (CCs). At every time step, we define a contiguous area of the precipitation intensity that is equal to or greater than a prescribed threshold from the radar observations (Figure 2(a)). The minimum threshold is set to be 10 mm h^{-1}, corresponding to about 40 dBZ from the reflectivity-rainfall intensity relationship used by JMA, in order to extract convective regions. The threshold of 40 dBZ, which was used by Steiner *et al.* (1995) and Geerts (1998) to identify convective echoes, is modified from the

original AITCC algorithm that uses the threshold of 30 dBZ (Shimizu and Uyeda 2012). If the contiguous area is equal to or greater than 200 km^2, the precipitation area is defined as a CC (Figure 2(b)). In most cases, multiple CCs are extracted at every time step. These extracted CCs are labeled with different identification numbers (ID) as shown in Figure 2(b).

The second procedure is to identify quasi-stationarity of CCs. Here we track the extracted CCs in time series and identify the lifetime of the QSCCs (Figure 2(c) and 2(d)). Figure 2(c) schematically depicts the centroids and defined areas of two CCs: one at time t = T; and the other at t = T + dt (dt: the time difference). From these CCs, an overlapped-area is determined by the areas of the CCs at t = T and t = T + dt (Figure 2(d)). At the same time, a motion vector is defined by pointing the centroid of the CC at t = T + dt from that of the CC at t = T (Figure 2(c)). Figure 2(d) displays the case where a part of the CC at t = T and a part of the CC at t = T + dt are overlapped. The magnitude of motion vector and the size of an overlapped area are used to determine the identity of a CC. The threshold of the maximum motion vector and the minimum overlapped area were set to be 16.7 m s^{-1} and 1 km^2 (corresponds to 1 grid point in the 1-km horizontal resolution of the radar data), respectively, in the original algorithm of Shimizu and Uyeda (2012). The threshold for the motion vector is changed to 10 m s^{-1} in the present study. Thus, if the magnitude of the motion vector is equal to or smaller than 10 m s^{-1}, the CC at t = T + dt is regarded as the same system with the CC at t = T. In this way, QSCCs are defined.

When a CC at t = T has multiple candidates at t = T + dt in this tracking procedure, a single CC that is the most likely linked to the CC at t = T is determined with the tracking algorithm of AITCC (see details in section 2.4 of Shimizu and Uyeda 2012). When a CC at t = T has

no candidate CCs at t = T + dt, the tracking algorithm stops. This time t = T is defined as the end of the lifetime of a QSCC. Here, the QSCCs whose lifetime is less than 20 minutes are excluded, because the lifetime should be resolved by at least three time steps of the radar data.

A possible limitation of the present method is that the method is not able to track a CC which propagates discretely; if there are no overlapping areas of CCs at t = T and t = T + dt, the CCs are not classified as the same CC. This limitation may bias the results toward shorter lifetimes.

[Figure 2 about here.]

2.3. *Environmental indices and parameters*

Environmental conditions before the development of the extracted QSCCs are investigated with the use of upper-air sounding data. For each QSCC, a sounding station which is within the 200 km range from and the nearest to the centroid of the QSCC is used. The atmospheric conditions at times within 1–9 hours prior to the developments of the extracted QSCCs are defined as the environments before the QSCC occurrence; the sounding data at these times are used for the present analysis. In other words, we do not use data at 0–1 hour and 10–11 hour before the QSCC development, because the data at 0–1 hour before may strongly be affected by QSCCs themselves and the data at 10–11 hour before may not reflect the environments before the development of QSCCs.

The environmental conditions are diagnosed in terms of indices and parameters related to static stability and vertical wind shear. There are a number of environmental indices and parameters that are related to stability and shear conditions (e.g., Markowski and Richardson 2010). The parameters examined here are convective available potential energy (CAPE),

convective inhibition (CIN), precipitable water (PW), Showalter Stability Index (SSI), K Index (KI) (George 1960), temperature lapse rate from 850 to 500 hPa (TLR) (Takemi 2007a,b), 0–3 km mean shear (MS03) (Rasmussen and Blanchard 1998), and 0–3 km environmental helicity (EH03) (Davies-Jones 1984). CAPE is calculated by adiabatically raising a parcel whose properties are vertically averaged in the lowest 500 m; in calculating CAPE the effects of condensate loading, entrainment, and latent heat of fusion are neglected, and buoyancy is defined with virtual temperature. In cases when the level of free convection is not identified, the values of CAPE and CIN are not obtained and hence not used for the statistical analyses described later. Choosing the 850-hPa and 500-hPa levels for the TLR calculation is based on an idea of comparing the effects of lapse rate and moisture in the definition of KI. The environmental property of EH03 is used to see how large the hodograph curvature is.

Another important factor for the development of QSCCs is a lifting effect. However, we do not address the lift due to the limitation of the radiosonde observations, which indicates the difficulty in estimating large-scale lifting from a single sounding.

For the purpose of comparing the environmental conditions before the development of the extracted QSCCs, environmental conditions for no-rain cases are also examined. The no-rain cases are defined as having no radar-observed precipitation at any grid points within the 200-km distance from the radiosonde sites between the observation times. It should be noted that once a radiosonde observation is associated with a certain QSCC, it is no longer used for other QSCCs or a no-rain case. A single observation is only used once and counted only once for the

composite. Statistical significance of the differences of the environmental parameters between the QSCCs and the no-rain cases is also examined[1].

3. Results

3.1. General characteristics of the extracted QSCCs

In this subsection, we will present overall characteristics of the extracted QSCCs. The total number of the extracted QSCCs are 4,133, while the total number of no-rain cases for a comparison purpose is 99,673[2].

The frequency distribution of the temporal and spatial means of precipitation intensity averaged for all the QSCCs is shown in Figure 3. Note that by definition the minimum value of the mean precipitation intensity is 10 mm h^{-1} (see section 2.2). A peak in the frequency distribution is seen at 20 mm h^{-1}, while the mean, median, and maximum values are 22.3, 21.5 and 54.0 mm h^{-1}, respectively. The frequency of the averages of precipitation intensity that is equal to or smaller than 30 mm h^{-1} is 93%.

[Figure 3 about here.]

Figure 4 shows the frequency distribution of the temporal mean of precipitating area for all the QSCCs averaged during their lifetimes. By definition the minimum value is 200 km^2. The frequency decreases with the increase in the precipitation area. Because of the shape of the distribution, the mean and median values are different with each other: 329 and 286

[1]Student's t-test is used to show the statistical significance in this study. If a distribution shows the one tail, Mann–Whitney U test will be additionally applied.

[2]This number means the number of the detected events on the radar data. Note that the actual total number for the no-rain environments is reduced to 7,619 (see details Figure 8 and the related descriptions).

km^2, respectively. The number of events with a large precipitation area becomes significantly reduced; the upper limit of the mean precipitation area identified in this analysis is 3,961 km^2. If these areas are assumed to have a circular shape, the mean and the maximum radius equivalent to a circle is about 10 km and 36 km, respectively. Thus, it can be assumed that typical sizes of the QSCCs with a circular shape assumed are about 20 km on average and 72 km at the maximum. The examination of the sizes of the extracted QSCC at all the time steps indicated that the maximum QSCC area is 10,616 km^2, which is one fifth of a mesoscale convective complex (e.g., Maddox 1980) of 50,000 km^2 with the threshold of temperature that is less than or equal to -52 degree C as a typical cloud area. This maximum area corresponds to the equivalent radius of 58 km, which indicates that the maximum horizontal size of QSCCs is about 120 km. Therefore, it is simply stated that the QSCCs in Japan are meso-β-scale phenomena. The horizontal scale of the QSCCs at their mean is smaller than that of a typical MCS, i.e., meso-α-scale (Glickman 2000). This is considered to be related to their shear environments, which will be examined in sections 3.4 and 3.5.

[Figure 4 about here.]

Examining the lifetimes of QSCCs indicates that the frequency of QSCCs lognormally decreases with the increase in the lifetime (Figure 5). Ninety five percent of the extracted QSCCs have a lifetime of less than 60 minutes. There is a slight change in the slope of the distribution at around the lifetime of 60 minutes. This means that a number of QSCCs with a longer lifetime becomes rapidly reduced.

[Figure 5 about here.]

The spatial distribution of the occurrence of QSCCs is shown in Figure 6(a). The location of each QSCC is defined as a point at which the QSCC is initially identified during the tracking procedure. A number of events is assessed in a unit area of 50 km by 50 km in order to see general characteristics by filtering out small-scale features. It is seen that QSCCs occur frequently on the Pacific side of the Japanese islands and the western part of Japan. Frequent occurrence is also seen on the Japan Sea side and the inland regions in central Japan. The frequency is generally lower in northern Japan than in the other regions. By comparing the spatial pattern in Figure 6(a) with terrain feature (Figure 1(a)), we can also note that overall the points with the frequency of greater than or equal to 30 correspond well to regions with high elevation and/or near mountainous topography.

To see how the amount of rainfall induced by QSCCs contributes to the total amount of rainfall during the warm season, the percentage of the total rainfall due to the extracted QSCCs to the total amount of rainfall during the warm season is examined and is shown in Figure 6(b). The percentage is seen to be higher in the western part and the Pacific side of the Japanese islands. In particular, higher values of greater than 3% are found over Kyushu, the southwestern part of Shikoku, the southern part of Kinki, and the north and the northwestern part of Kanto. The spatial distribution of the occurrence of the QSCCs may be associated with a regional feature of the environmental parameters, which will be mentioned in section 3.3.

Based on Figure 6, the whole analysis region of Japan is divided into three regions. The first region is the Hokkaido region, where both the frequency and the rainfall contribution of QSCCs are the lowest. Regions with higher frequency are divided into the Japan Sea side region, and the Pacific side region. The radiosonde sites in the Hokkaido region are WKN,

SPR, KSR, and NMR; those in the Japan Sea side region are AKT, WJM, YNG, and MTE; and those in the Pacific side region are TTN, HMT, SNM, FKO, and KGS. As a representation of each region, the stations of SPR, AKT, and KGS are chosen for the Hokkaido, the Japan Sea side, and the Pacific side region, respectively (e.g., Chuda and Niino 2005). By dividing the whole analysis area in this way, the environmental conditions for the QSCC development are examined, which will be described in section 3.2.

[Figure 6 about here.]

The temporal change of the QSCC characteristics during the warm season is investigated as a monthly basis. Figure 7 exhibits the monthly changes in the total numbers of the QSCCs. The number of the QSCCs exceeds 500 from July to September, having a peak in August, while that in May and October becomes largely reduced. The higher frequency of the QSCCs is considered to be due to Asian monsoon activity (rainy season) in June and July, and eventual tropical cyclones and stationary fronts from August to September. One thing to be noted here is that, the rainbands associated with tropical cyclones are included in the extracted QSCCs in this study, because we investigate various types of convection.

[Figure 7 about here.]

To show how frequent rainfall events occur during the warm season, we examine the percentage of the number of no-rain cases to the total number of the radiosonde observation times. Figure 8 shows the month-to-month change of this no-rain percentage as well as the actual number of no-rain cases. In contrast to the features found in Figure 7, it is seen from Figure 8 that the percentage and the actual number of the no-rain cases are lower from July to

September, while that is the highest in May. Although the features of June and October seem to be similar, the occurrence of QSCCs is lower in October than in June (Figure 7).

[Figure 8 about here.]

Based on the monthly features shown in Figures 7 and 8, the warm season from May to October is categorized into three sub-seasons. May and October are in spring and autumn, respectively, and are summarized as the same sub-season, referred to as Season 1 (denoted as S1). June, which belongs to a rainy season because of the higher activity of Asian monsoon, is defined as Season 2 (hereafter S2). July-August-September is defined as Season 3 (hereafter S3). Based on this categorization, the environmental properties of QSCCs are investigated in the following section.

3.2. Vertical structure of the environmental atmosphere

In this subsection, we examine the vertical structure of the environmental atmosphere for the development of the extracted QSCCs (denoted as Q category) by comparing with those for the no-rain cases (denoted as N category). Hereafter, the Q and N categories are referred to as Q and N. The vertical profiles of SPR, AKT, and KGS are averaged in each season, i.e., S1, S2, and S3.

Firstly, the characteristics of the vertical profiles of temperature, moisture, and wind are described to provide overall views for the stability and shear conditions that will be given in the next subsection. The vertical profiles of temperature, water vapor mixing ratio, and relative humidity for Q and N are shown in Figure 9. A common feature found in the temperature profiles is that temperatures under the level of 850 hPa and above the level of 400 hPa are

higher in Q than in N for all the three sites in all the seasons (Figures 9(a), 9(d), 9(g)), which are statistically significant at a confidence level of 95% (Figures 10(a), 10(d), 10(g)). On the other hand, temperatures at the middle levels do not show a consistent feature between Q and N, although they are a little higher in Q than in N. Note that the T-values at the 600- and 700-hPa levels are smaller, which suggests that the statistical significance of the difference may be marginal. The smaller T-values at the middle levels are also seen in HMT, MTE, and YNG in the season of S3 (see Figures SI-6(d) and SI-7(d) of Supporting Information).

In contrast to the temperature profiles, the difference of water vapor mixing ratio and relative humidity between the categories is clearly identified. Water vapor mixing ratio and relative humidity throughout the troposphere are higher in Q than in N for all the three sites in all the seasons (Figures 9(b), 9(c), 9(e), 9(f), 9(h), 9(i)). The differences described above are also statistically significant at a confidence level of 95% (Figure 10(b), 10(c), 10(e), 10(f), 10(h), 10(i)). On the other hand, there are no significant differences of the water vapor mixing ratio between Q and N at the lower and upper troposphere in S2 of SPR (Figure 10(b)). This feature is also seen in WKN in the seasons of S1 and S2 (see Figures SI-1(b)–(c) and SI-5(b)–(c) of Supporting Information). Considering these features, it should be noted that the environments for the development of QSCCs are characterized as both higher temperature at the lower troposphere and larger moisture throughout the troposphere during the warm season in Japan. These differences of temperature and moisture between the categories will affect the diagnosis of stability conditions, which will be described in the next subsection.

[Figure 9 about here.]

[Figure 10 about here.]

The features of the wind profiles can be obtained from the hodographs. Figure 11 compares the mean wind hodographs in Q and N depending on the site and the season. The differences in the shapes of the hodograph between the categories are clearly seen. The shapes in Q indicate a clockwise veering feature from the surface to about 700 hPa and a nearly unidirectional structure above that level. On the other hand, in N, a wind veering is not seen at the lower levels, while slight anti-clockwise feature can be identified at the middle-to-upper levels in some sites/seasons. One of the pronounced features on the hodograph curvatures in Q is that easterly winds are seen at the lower troposphere at all the three sites (Figures 11(a)–(c)). This feature is mostly seen over the Pacific side in the season of S1, which is related to larger hodograph curvature in Q. In addition, the hodograph shapes and the direction of rotation strongly depend on the meridional wind at all the three sites in all the seasons. Most of these differences of zonal and meridional winds between Q and N are statistically significant at a confidence level of 95% (Figure 12), except for the zonal wind in the seasons of S1 and S2 (Figures 12(a), 12(c), 12(e)). The significant difference seen here corresponds to the difference of the hodograph curvature between Q and N. The statistical difference suggests that the clockwise veering in Q and the anti-clockwise veering in N control the shear condition for the development of QSCCs.

[Figure 11 about here.]

[Figure 12 about here.]

If the environmental winds are assumed to be geostrophic winds, there is warm advection associated with the clockwise veering feature in Q (in terms of thermal wind balance). In addition, the hodographs in Q are consistent with the environments on the warmer side of warm or stationary front, which is a common place for the development of convective systems (Laing and Fritsch 2000). Here, warm air advection is one of the forcing terms for ascent in the quasi-geostrophic approximated ω-equation, and thus it is suggested that the hodograph shape in Q is related with the large-scale ascent. Although other conditions (e.g., an intrusion of jet in the upper troposphere) are required to induce the large-scale ascent, one possibility for the existence of large-scale ascent is demonstrated from the hodograph.

Based on the analysis of the characteristics of the vertical profiles, the environmental properties for the development of QSCCs will be described with the use of some stability and shear indices that characterize environmental conditions in the following subsection. The comparison between Q and N will also be provided.

3.3. Diagnosis of conditions for the development of QSCCs with environmental parameters

As described in section 2.3, the environmental conditions for the development of QSCCs are diagnosed in terms of stability and shear parameters. A diagnosis with the use of these parameters is useful for identifying the differences of the environmental conditions between Q and N.

Figure 13 shows the frequency distributions of the environmental parameters in Q and N. To see general characteristics of the environmental parameters throughout Japan, all the data

shown in Figure 13 are composited for all the analysis sites. Except for TLR, the differences of the parameters between Q and N are clearly seen. Compared to N, Q indicates a larger amount of PW, a higher degree of instability (SSI, KI, and CAPE), and stronger shear (MS03) with a larger hodograph curvature (EH03). Considering that there is a large difference of PW while little difference of TLR between the categories, the moisture difference seems to control the differences seen for other stability parameters as indicated by SSI (see Eq. (1) in Appendix), KI (see Eq. (2) in Appendix), and CAPE.

From the analyses of vertical profiles of moisture, it was found that the moisture is larger in Q than in N throughout the troposphere. Considering that SSI, KI, and CAPE become larger with a larger amount of moisture content in the lower troposphere and that temperature lapse rate was indicated to be near saturated neutral (moist adiabatic), it is suggested that the amount of moisture in the lower layer controls the stability condition for the QSCCs.

[Figure 13 about here.]

Table 1 summarizes the averages and standard deviations of those environmental parameters[3]. Statistical significance of the differences of the mean values between Q and N is examined with the test statistic T. Table 1 also shows the values of test statistic T for the environmental parameters. As expected from the features seen in Figure 13, it is found that all the environmental parameters except TLR indicate a significant difference between Q and N. Overall the T values pronouncedly exceed the significance level, and the T values for PW and KI are the highest ones among the parameters. Because KI takes into account the effects of moisture at the levels of 850 and 700 hPa (see Eq. (2) in Appendix), the higher

[3]To see the values of CAPE, PW, SSI, and MS03 for the QSCCs at all the sites and all the seasons, please see Tables SI-1–SI-4 of Supporting Information.

value of T in KI seems to be due to the significant difference of PW that may also affect moisture at each vertical level. Therefore, the difference of the water vapor contents between Q and N is considered to control the environmental properties for the development of QSCCs rather than the difference of temperature lapse rate. The moisture content at each height will be discussed later in this subsection. As far as the kinematic parameters are concerned, both MS03 and EH03 indicate that there are significant differences between the categories. Thus, the magnitude and direction of wind shear in the lower troposphere also characterize the difference between Q and N.

[Table 1 about here.]

The distributions of CAPE, PW, and MS03, whose values are averaged during the warm season at each site, are shown in Figure 14 in order to see the regional features of environmental parameters. CAPE, PW, and MS03 are selected to examine stability, moisture, and shear conditions, respectively. The values of CAPE and PW mostly increase with the decrease in the latitude. The regional feature of CAPE is consistent with the previous findings of Chuda and Niino (2005). In contrast, the values of MS03 are larger in the Hokkaido region and in the southern part of Japan (SNM and KGS) ($> 13.0 \times 10^{-4}$ s^{-1}) than in the middle of Japan (TTN, HMT, MTE, YNG, and FKO) ($< 13.0 \times 10^{-4}$ s^{-1}). Compared with Figure 6, larger populations of QSCCs are mostly seen at locations with the larger values of CAPE and PW.

[Figure 14 about here.]

The seasonal and regional variations of the environmental parameters are further described here. Because of the significant differences between Q and N, the variations of the environmental conditions for QSCCs are examined by concentrating on PW and KI. Figure 15(a)–(c) shows the variation of the monthly mean PW and Figure 15(d)–(f) the monthly mean KI. Each panel in Figure 15 summarizes the variations for each region. Both PW and KI unanimously indicate higher values in Q than in N at all the locations in all the months. In other words, the significant differences found in the overall averages shown in Table 1 are consistently seen throughout the regions during the warm season. The variations of PW and KI during the months show that highest values are generally seen in July and August in Q. The PW and KI values take lowest values in May and October.

[Figure 15 about here.]

The results described above show that the moisture content is the most distinguishing factor in characterizing the environmental conditions for the development of QSCCs from no-rain cases among the stability parameters. Although PW is found to be an important parameter, the levels at which moisture content contributes to PW are not known. Because it was found that middle-level humidity plays important roles in controlling the structure and intensity of cumulus convection and MCSs (Takemi *et al.* 2004; Derbyshire *et al.* 2004; Takemi 2007a; Takemi 2014b; Takemi 2015), the moisture content at each vertical layer and its contribution to the total amount of moisture (i.e., PW) are examined here. For this purpose, the vertically integrated water vapor contents in vertical layers of a 1 km depth are computed. The vertically integrated water vapor contents from the height of X km to Y km are referred to as PW

followed by the bottom (X km) and top (Y km) heights; for example, the water vapor content vertically integrated from 0 to 1 km is referred to as PW01.

The differences of the layer-integrated moisture content between Q and N are compared in terms of frequency distribution. The moisture content in all the layers is consistently larger in Q than in N (not shown). In addition, the difference between the categories appears to be more pronounced with the increase in the height level. This result indicates that the environmental conditions for QSCCs are characterized by a larger amount of moisture at middle levels.

The importance of middle-level moisture content can also be found for the difference of the contribution of the layer-integrated moisture to the total amount of moisture, i.e., PW. Thus, we examined the contribution of the layer-integrated moisture content at each layer to PW (Figure 16). Compared with the difference of the frequency distributions between Q and N in the lower layers, the departure of the distribution in Q becomes more distinct from the N distribution with the increase in the layer height. Namely, the amount of moisture at middle levels largely contributes to precipitable water vapor in the environments of Q. Considering that PW is significantly larger in Q than in N, it is suggested that an increase in the middle-level moisture leads to a larger amount of PW for the development of the QSCCs.

The environmental condition with a larger amount of middle-level moisture was also identified for convective precipitation events in the afternoon during the summer over the plain regions (the metropolitan areas of Tokyo and Nagoya) facing to the Pacific in Japan (Nomura and Takemi 2011; Takemi 2014a). The present analysis is consistent with these previous findings. Therefore, a larger amount of moisture is considered to a common feature that distinguishes the environments for the development of not only summertime thunderstorms

but also organized convective systems during the warm season in Japan. One thing to be noted here is that, a larger middle-level moisture controls the convective development over the tropics (Takemi *et al.* 2004; Kikuchi and Takayabu 2004), and the western part of Kyushu Island (Kato 2006). At the mature stage of the quasi-stationary convective systems, the moisture at the middle-level controls the development associated with the convective systems (Kato 2006): the wet (dry) environment at the middle-level troposphere gives a condition favorable (unfavorable) for the development of convective systems. Considering that the larger middle-level moisture controls the development of convection, it is emphasized that atmospheric moistening before the development stage of convection plays an important role in the development of the QSCCs.

[Figure 16 about here.]

3.4. Relationships between environmental conditions and rainfall characteristics

In the previous subsection, the environmental properties for the development of the QSCCs were investigated through the comparison of those in the no-rain cases. Differences in the environmental properties between the QSCC occurrence and the no-rain cases were demonstrated. In this subsection, the dependence of the intensity and area of rainfall produced by QSCCs on the environmental conditions is investigated.

Figure 17 shows the relationships between the averaged precipitation intensity within the identified QSCCs and the environmental parameters. The correlation coefficients between the precipitation intensity and the parameters are also indicated. Although the correlation coefficients are small, positive (negative) relationships of the precipitation intensity with the

thermodynamic parameters are found for CAPE, CIN, and TLR (SSI). The relationships between the precipitation intensity and the parameters CAPE, SSI, and TLR are reasonable, because stronger instability is related to stronger precipitation intensity. For the shear parameters (i.e., MS03 and EH03), there are negative relationships between the precipitation intensity and the parameters. In terms of the correlation coefficient, the relationships of the precipitation intensity with CAPE, SSI, TLR, and MS03 indicate higher correlation.

The relationships between the precipitation area of the QSCCs and the environmental parameters are demonstrated in Figure 18. In contrast to the case of the precipitation intensity, the relationships between the precipitation area and the thermodynamic parameters seem to be inconsistent with convective instability concept. In general, the correlation coefficients between the precipitation area and the thermodynamic parameters are negligible. On the other hand, the relationships with the shear parameters indicate that there is a positive and higher correlation of the precipitation area with the shear parameters. The highest correlation is seen for the relationship with MS03.

From this analysis on the relationship between the precipitation characteristics and the environmental parameters, it is found that higher convective instability is related to stronger precipitation intensity while stronger vertical shear to larger precipitation area. Therefore, it can be stated that convective instability has the strongest correlation with precipitation intensity within the QSCCs and shear intensity is associated with the size of the precipitation area.

[Figure 17 about here.]

[Figure 18 about here.]

3.5. *Characteristics of slower- and faster-moving systems*

In this study, we have focused on convective clusters whose motion speed is less than or equal to 10 m s^{-1}, which we regard as quasi-stationary. However, the speed of about 10 m s^{-1} may not be small; for example, Barnes and Sieckman (1984) termed a mesoscale convective cloud line whose motion speed is greater than 7 m s^{-1} as a fast-moving line. Thus, in this subsection, we examine and compare the characteristics between slower-moving and faster-moving CCs.

Figure 19 shows the frequency distribution of the motion speed of the extracted QSCCs. A peak frequency is found at the speed of 6.0 m s^{-1}, and the mean speed, v_{mean}, is 5.6 m s^{-1}, indicating that the shape of the frequency distribution looks normal despite a little shift to higher values. Thus, we divide the QSCCs into two sub-categories: slower-moving and faster-moving CCs depending on their motion speed in order to show the differences in the characteristics between slower-moving and faster-moving CCs. Slower-moving CCs (denoted as S) are defined as clusters whose motion speed is less than $v_{\mathrm{mean}} - 1\sigma$, while faster-moving CCs (denoted as F) as clusters whose motion speed is greater than $v_{\mathrm{mean}} + 1\sigma$, where standard deviation of the motion speed of the extracted QSCCs, σ, is 1.8 m s^{-1}. Hereafter, the S and F categories are referred to as S and F. Here, the total numbers of S and F are 706 and 718 among the 4,133 QSCCs, respectively.

[Figure 19 about here.]

Firstly, the statistics of the temporal and spatial means of precipitation intensity and the temporal mean of precipitation area for each category are shown in Figure 20. Figure 20 shows the maxima/minima, medians, and 75 and 25 percentiles. Precipitation intensity is larger in S than in F (Figure 20(a)), while precipitation area is smaller in S than in F (Figure 20(b)). The examination of the statistical significance of the differences in the means between the two categories indicates that precipitation intensity is significantly larger in S than in F, while precipitation area is significantly smaller in S than in F at the 95% confidence level. Therefore, it is found that the slower-moving CCs have a stronger intensity and a smaller horizontal size of precipitation than the faster-moving CCs.

[Figure 20 about here.]

To see how the difference of the distributions in Figure 20 arises from a viewpoint of the environmental properties, Figure 21 compares the frequency distributions of the environmental parameters in S and F. Compared to F, S indicates a smaller amount of PW, a higher degree of instability (SSI, TLR, and CAPE), and weaker shear (MS03) with a smaller hodograph curvature (EH03).

[Figure 21 about here.]

Statistical significance of the differences of the mean values between S and F is examined with the test statistic T. Table 2 shows the values of test statistic T for the environmental parameters. All the environmental parameters indicate statistically significant differences between S and F. It is seen that the S environment shows higher instability (SSI, TLR, and CAPE) and weaker shear (MS03 and EH03), but lower moisture (PW) than the F environment.

[Table 2 about here.]

The monthly changes of CAPE, PW, and MS03, respectively, are shown in Figure 22 with the same reason as described in section 3.3 and shown in Figure 14. CAPE (MS03) is clearly larger (smaller) in S than in F, in a consistent manner with those shown in Figure 21 and Table 2, while PW has a larger monthly variation in F than in S. Thus, it is suggested that there are no consistent features in the PW variation on the monthly basis.

We will describe again the relationships between environmental conditions and rainfall characteristics, but for S and F. Overall features for the precipitation intensity between S and F are the same as those between Q and N. This suggests that the environmental conditions for the slower-moving CCs are characterized by higher instability and weaker vertical shear. In contrast to the precipitation intensity, there are no discernible relationships between precipitation area and the environmental parameters (not shown).

[Figure 22 about here.]

From the analyses of environmental parameters for S and F, the physical interpretation of the results of Figures 20 and 21 are attempted here. Firstly, from the analyses of the relationships between environmental conditions and rainfall characteristics, it was found that the larger precipitation intensity is related to higher instability and to weaker shear intensity. The bulk Richardson number in S, estimated by using CAPE and a shear between the levels of 0 and 6 km (Table 2), is about 100, which corresponds to a condition for the development of multicell storms (Weisman and Klemp 1982). Because the CAPE values for Q are considerably smaller than those for squall lines and supercell storms over the Great Plains of the United States

(Bluestein and Jain 1985), stronger shears are detrimental to the development of convection even in the multicell category in terms of bulk Richardson number. Thus, the moderate value of the vertical wind shear is appropriate for the development of the slower-moving CCs, a type of multicell storms, in Japan.

It is noted that the smaller precipitation area in the slower-moving CCs associated with smaller MS03 can be attributed to the fact that the shape of shear determines the organization mode of MCSs (LeMone *et al.* 1998; Parker and Johnson 2000). A stronger environmental shear is in general favorable for a more organized structure on MCSs (e.g., Weisman and Rotunno 2004). In addition, the environmental shear also restricts the size and motion of convective cells within MCSs (e.g., Doswell *et al.* 1996). In other words, a weaker shear is detrimental for the organization of convection. Therefore, it is considered that a weaker shear condition identified for the slower-moving CCs leads to less organized and smaller CCs.

4. Summary and conclusions

The characteristics and environmental properties of QSCCs during the warm season in Japan were statistically investigated using weather radar and upper-air sounding data of JMA from May to October during 2005–2012. An algorithm developed by Shimizu and Uyeda (2012), called AITCC, was modified to identify QSCCs from radar data. We found 4,133 QSCCs over the Japanese major islands.

Compiling numerous QSCC samples revealed that the horizontal scales of QSCCs on average and at the maximum with a circular shape are about 20 km and 72 km, respectively. Thus, QSCCs in Japan are regarded as meso-β-scale phenomena. Ninety-five percent of

the extracted QSCCs have a lifetime of less than 60 minutes, and the number of longer-lived QSCCs rapidly decreases as the lifetime increases. QSCCs occur more frequently on the Pacific side of the Japanese islands and the inland regions in central Japan, which are associated with higher convective instabilities, more moisture, and intermediate shear intensities.

The analyses of the vertical profiles of temperature, water vapor mixing ratio, and horizontal winds between the QSCC case and no-rain case indicate that the temperatures below the 850-hPa level and above the 400-hPa level are larger in the QSCC case than in the no-rain case. It is also indicated that the moisture content throughout the troposphere is larger in the QSCC case than in the no-rain case. The shear profile indicates that there are pronounced differences in the meridional component between the QSCC and the no-rain cases; there is a southerly component in the QSCC cases and a northerly component in the no-rain cases, suggesting that the hodograph shape in the QSCC cases is related with the large-scale ascent. Although other conditions (e.g., an intrusion of the jet in the upper atmosphere) are required to induce the large-scale ascent, one possibility for the existence of the large-scale ascent is demonstrated in this study.

The environmental conditions for the occurrence of the QSCCs were further investigated using stability and shear parameters. Most of the examined thermodynamic parameters indicate that there is a significant difference in the stability condition of the QSCC and no-rain cases. The moisture contents not only at the lower levels but also at the middle levels (above the 2-km height) are significantly larger in the QSCC condition than in the no-rain condition. This moisture difference leads to differences in KI, SSI, and PW between the QSCC

and no-rain cases. The kinematic parameters indicated that both MS03 and EH03 significantly characterize the environmental conditions of the QSCC cases from the no-rain cases. From the diagnosis using the environmental indices, it is concluded that the amount of moisture in the lower layer controls the stability condition for the development of the QSCCs, and that the magnitudes of the wind shear and the helicity at the lower levels distinguish the kinematic environment for the development of the QSCCs.

In addition, the moisture content at each vertical level and its contribution to the total amount of moisture (i.e., PW) were also examined. An increase in the middle-level moisture leads to more PW in the QSCC environments. Considering that a larger middle-level moisture controls the development of convection (Takemi *et al.* 2004; Kikuchi and Takayabu 2004; Derbyshire *et al.* 2004; Kato 2006; Takemi 2015), atmospheric moistening before the development stage of convection plays an important role in the development of the QSCCs.

Examining the relationship between the precipitation intensity/area of the QSCCs and the environmental parameters shows that the precipitation intensity is more strongly correlated with CAPE and SSI, while the precipitation area is more highly correlated with MS03. Simply stated, the statistical analyses of numerous QSCCs samples extracted from the long-term data reveal that the precipitation intensity within the QSCCs during the warm season in Japan has a higher correlation with the convective instability while the precipitation area has a stronger correlation with the shear intensity.

The characteristics and environmental properties between slower- and faster-moving CCs were compared. Investigating the statistical significance of the differences in the means between the two categories indicates that the precipitation intensity is significantly larger in

slower-moving CCs than in faster-moving CCs, while the precipitation area is significantly smaller in the slower-moving CCs. The analysis of environmental parameters suggests that the stronger precipitation intensity for the slower-moving CCs is due to a higher instability and a weaker shear intensity, whereas the smaller precipitation area is due to a weaker shear intensity.

QSCCs are widespread mesoscale phenomena not only in Japan but also around the world. In generating QSCCs, a complex topography should play an important role. A complex terrain characterizes the geographical features in Japan; and therefore the geographical features should have a significant impact on the occurrence of QSCCs. In addition, moister conditions characterize the environmental settings for the occurrence of QSCCs in humid-climate regions. From the numerical experiments conducted by Takemi (2014b), moister environments lead to the development of stronger and more organized CCs. The present study shows that middle-level moister conditions favor the occurrence of stronger precipitation intensity within the QSCCs. These results should contribute to the understanding of quasi-stationary or slow-moving convective clusters in those regions.

Furthermore, the present study demonstrates that operational data such as radars, upper-air soundings, and high-resolution gridded analyses provided by meteorological centers are very useful for investigating mesoscale convective phenomena and their environmental properties from a climatological point of view. Although we have previously conducted this type of study using operational meteorological data (Nomura and Takemi 2011; Takemi 2014a), the present study also confirms the usefulness of this approach. The outcome from our studies should provide basic information on the diagnosis of mesoscale phenomena.

Acknowledgements

We would like to thank Dr. Shingo Shimizu at National Research Institute for Earth Science and Disaster Prevention who provided us the program of Algorithm for the Identification and Tracking of Convective Cells (AITCC). The constructive comments and suggestions by two anonymous reviewers and the editor-in-charge, Prof. Douglas J. Parker, are greatly acknowledged for improving the original manuscript. The operational radar dataset used in this study was provided by Japan Meteorological Business Support Center. The upper-air sounding data used in this study were obtained from the "Atmospheric Soundings" web site (`http://weather.uwyo.edu/upperair/sounding.html`) at the University of Wyoming. Convective available potential energy was calculated using the Fortran90 program obtained from the website of Dr. George H. Bryan at National Center for Atmospheric Research. The Generic Mapping Tools, GMT, was used for drawing some of the figures.

Appendix: Definition of SSI and KI

To assist the discussion on the relationships between the thermodynamic-vertical profiles and environmental properties in the sections from 3.2 to 3.5, we will describe the definition of Showalter Stability Index (SSI) and K Index (KI) as follows;

$$SSI = T_{500} - T^{*}_{850\rightarrow 500}, \quad (1)$$

$$KI = T_{850} - T_{500} + T_{d850} - (T_{700} - T_{d700}), \quad (2)$$

where T_{850}, T_{700}, and T_{500} are the temperature at the 850, 700, and 500 hPa level, respectively. T_{d850} and T_{d700} are the dew-point temperature at the 850 hPa and 700 hPa, respectively, and

$T^*_{850\to500}$ is the 500-hPa temperature whose property is adiabatically lifted from 850 hPa to 500 hPa.

References

Anquetin S, Minsicloux F, Creutin JD, Cosma S. 2003. Numerical simulation of orographic rainbands. *J. Geophys. Res.*, **108:** D88386, DOI: 10.1029/2002JD001593.

Barnes GM, Sieckman K. 1984. The environment of fast- and slow-moving tropical mesoscale convective cloud lines. *Mon. Wea. Rev.*, **112:** 1782–1794, DOI: 10.1175/1520-0493(1984)112<1782:TEOFAS>2.0.CO;2.

Bluestein HB, Jain MH. 1985. Formation of mesoscale lines of precipitation: Severe squall lines in Oklahoma during the spring. *J. Atmos. Sci.*, **42:** 1711–1732, DOI: 10.1175/1520-0493(1987)115<2719:FOMLOP>2.0.CO;2.

Buzzi A, Foschini L. 2000. Mesoscale meteorological features associated with heavy precipitation in the Southern Alpine region. *Meteorol. Atmos. Phys.*, **72:** 131–146, DOI: 10.1007/s007030050011.

Chappell CF. 1986. Quasi-stationary convective events. In *Mesoscale Meteorology and Forecasting*. Ray PS. (ed.) 289–310. Amer. Meteorol. Soc: Boston, MA.

Chuda T, Niino H. 2005. Climatology of environmental parameters for mesoscale convections in Japan. *J. Meteor. Soc. Jpn*, **83:** 391–408, DOI: 10.2151/jmsj.83.391.

Davolio S, Buzzi A, Malguzzi P. 2009. Orographic triggering of long lived convection in three dimensions. *Meteorol. Atmos. Phys.*, **103:** 35–44, DOI: 10.1007/s00703-008-0332-5.

Davies-Jones RP. 1984. Streamwise Vorticity: The origin of updraft rotation in supercell storms. *J. Atmos. Sci.*, **41:** 2991–3006, DOI: 10.1175/1520-0469(1984)041<2991:SVTOOU>2.0.CO;2.

Derbyshire SH, Beau I, Bechtold P, Grandpeix JY, Piriou JM, Redelsperger JL, Soares PMM. 2004. Sensitivity of moist convection to environmental humidity. *Q. J. R. Meteorol. Soc.*, **130:** 3055–3079, DOI: 10.1256/qj.03.130.

Doswell CA, Brooks HE, Maddox RA. 1996. Flash flood forecasting: An ingredients-based methodology. *Wea. Forecasting*, **11:** 560–581, DOI: 10.1175/1520-0434(1996)011<0560:FFFAIB>2.0.CO;2.

Geerts B. 1998. Mesoscale convective systems in the Southeast United States during 1994–95: A survey. *Wea. Forecasting*, **13:** 860–869, DOI: 10.1175/1520-0434(1998)013<0860:MCSITS>2.0.CO;2.

George JJ. 1960. *Weather forecasting for aeronautics*. Academic Press: New York; pp. 673.

Glickman TS (ed). 2000. *Glossary of Meteorology*, 2nd edition. American Meteorological Society: Boston; pp. 855.

Hirockawa Y, Kato T. 2012. Kinetic energy budget analysis on the development of a meso-β-scale vortex causing heavy rainfall, observed over Aomori Prefecture in Northern Japan on 11 November 2007. *J. Meteor. Soc. Jpn*, **90:** 905–921, DOI: 10.2151/jmsj.2012-604.

Kato T. 1998. Numerical simulation of the band-shaped torrential rain observed over Southern Kyushu Japan on 1 August 1993. *J. Meteor. Soc. Jpn*, **76:** 97–128.

Kato T. 2005. Statistical study of band-shaped rainfall systems the Koshikijima and Nagasaki lines observed around Kyushu Island Japan. *J. Meteor. Soc. Jpn*, **83:** 943–957, DOI: 10.2151/jmsj.83.943.

Kato T. 2006. Structure of the band-shaped precipitation system inducing the heavy rainfall observed over northern Kyushu, Japan on 29 June 1999. *J. Meteor. Soc. Jpn*, **84:** 129–153, DOI: 10.2151/jmsj.84.129.

Kato T, Aranami K. 2005. Formation factors of 2004 Niigata-Fukushima and Fukui heavy rainfalls and problems in the predictions using a cloud-resolving model. *SOLA*, **1:** 1–4, DOI: 10.2151/sola.2005-001.

Kato T, Goda H. 2001. Formation and maintenance processes of a stationary band-shaped heavy rainfall observed in Niigata on 4 August 1998. *J. Meteor. Soc. Jpn*, **79:** 899–924, DOI: 10.2151/jmsj.79.899.

Kikuchi K, Takayabu YN. 2004. The development of organized convection associated with the MJO during TOGA COARE IOP: Trimodal characteristics. *Geophys. Res. Lett.*, **31:** L10101, DOI: 10.1029/2004GL019601.

Laing AG, Fritsch JM. 2000. The large-scale environments of the global populations of mesoscale convective complexes. *Mon. Wea. Rev.*, **128:** 2756–2776, DOI: 10.1175/1520-0493(2000)128<2756:TLSEOT>2.0.CO;2.

LeMone MA, Zipser EJ, Trier SB. 1998. The role of environmental shear and thermodynamic conditions in determining the structure and evolution of mesoscale convective systems during TOGA COARE. *J. Atmos. Sci.*, **55:** 3493–3519, DOI: 10.1175/1520-0469(1998)055<3493:TROESA>2.0.CO;2.

Maddox RA. 1980. Mesoscale convective complexes. *Bull. Amer. Meteor. Soc.*, **61:** 1374–1387, DOI: 10.1175/1520-0477(1980)061<1374:MCC>2.0.CO;2.

Markowski P, Richardson Y. 2010. *Mesoscale meteorology in midlatitudes*. Wiley-Blackwell: pp. 407.

Meng Z, Yan D, Zhang Y. 2013. General features of squall lines in East China. *Mon. Wea. Rev.*, **141:** 1629–1647, DOI: 10.1175/MWR-D-12-00208.1.

Nomura S, Takemi T. 2011. Environmental stability for afternoon rain events in the Kanto Plain in summer. *SOLA*, **7:** 9–12, DOI: 10.2151/sola.2011-003.

Ogura Y. 1991. Analysis and mechanism of intense precipitation. *Tenki*, **38:** 276–288 (in Japanese).

Orlanski I. 1975. A rational subdivision of scales for atmospheric processes. *Bull. Am. Meteorol. Soc.*, **56:** 527–530.

Panziera L, James CN, Germann U. 2014. Mesoscale organization and structure of orographic precipitation producing flash floods in the Lago Maggiore region. *Q. J. R. Meteorol. Soc.*, **141:** 224–248, DOI: 10.1002/qj.2351.

Parker MD, Johnson RH. 2000. Organizational Modes of Midlatitude Mesoscale Convective Systems. *Mon. Wea. Rev.*, **128:** 3413–3436, DOI: 10.1175/1520-0493(2001)129<3413:OMOMMC>2.0.CO;2.

Rasmussen EN, Blanchard DO. 1998. A baseline climatology of sounding-derived supercell and tornado forecast parameters. *Wea. Forecasting*, **13:** 1148–1164, DOI: 10.1175/1520-0434(1998)013<1148:ABCOSD>2.0.CO;2.

Schumacher RS, Johnson RH. 2008. Mesoscale processes contributing to extreme rainfall in a midlatitude warm-season flash flood. *Mon. Wea. Rev.*, **136:** 3964–3986, DOI: 10.1175/2008MWR2471.1.

Shimizu S, Uyeda H. 2012. Algorithm for the identification and tracking of convective cells based on constant and adaptive threshold methods using a new cell-merging and -splitting scheme. *J. Meteor. Soc. Jpn*, **90:** 869–899, DOI: 10.2151/jmsj.2012-602.

Steiner M, Houze RA, Yuter SE. 1995. Climatological characterization of three-dimensional storm structure from operational radar and rain gauge data. *J. Appl. Meteor.*, **34:** 1978–2007, DOI: 10.1175/1520-0450(1995)034<1978:CCOTDS>2.0.CO;2.

Takemi T. 2007a. A sensitivity of squall line intensity to environmental static stability under various shear and moisture conditions. *Atmos. Res.*, **84:** 374–389, DOI: 10.1016/j.atmosres.2006.10.001.

Takemi T. 2007b. Environmental stability control of the intensity of squall lines under low-level shear conditions. *J. Geophys. Res.*, **112:** D24110, DOI: 10.1029/2007JD008793.

Takemi T. 2014a. Characteristics of summertime afternoon rainfall and its environmental conditions in and around the Nobi Plain. *SOLA*, **10:** 158–162, DOI: 10.2151/sola.2014-033.

Takemi T. 2014b. Convection and precipitation under various stability and shear conditions: Squall lines in tropical versus midlatitude environment. *Atmos. Res.*, **142:** 111–123, DOI: 10.1016/j.atmosres.2013.07.010.

Takemi T. 2015. Relationship between cumulus activity and environmental moisture during the CINDY2011/DYNAMO field experiment as revealed from convection-resolving simulations. *J. Meteor. Soc. Jpn*, in press, DOI: 10.2151/jmsj.2015-035.

Takemi T, Hirayama O, Liu C. 2004. Factors responsible for the vertical development of tropical oceanic cumulus convection. *Geophys. Res. Lett.*, **31:** L11109, DOI: 10.1029/2004GL020225.

Warren RA, Kirshbaum DJ, Plant RS, Lean HW. 2014. A 'Boscastle-type' quasi-stationary convective system over the UK Southwest Peninsula. *Q. J. R. Meteorol. Soc.*, **140:** 240–257, DOI: 10.1002/qj.2124.

Weisman ML, Klemp JB. 1982. The dependence of numerically simulated convective storms on vertical wind shear and buoyancy. *Mon. Wea. Rev.*, **110:** 504–520, DOI: 10.1175/1520-0493(1982)110<0504:TDONSC>2.0.CO;2.

Weisman ML, Rotunno R. 2004. "A Theory for Strong Long-Lived Squall Line" Revisited. *J. Atmos. Sci.*, **61:** 361–382, DOI: 10.1175/1520-0469(2004)061<0361:ATFSLS>2.0.CO;2.

Yoshizaki M, Kato T. 2007. *Meteorology of heavy rainfall and snowfall*. Asakura Publishing Co.: pp. 187 (in Japanese).

Yoshizaki M, Kato T, Tanaka Y, Takayama H, Shoji Y, Seko H. 2000. Analytical and numerical study of the 26 June 1998 orographic rainband observed in Western Kyushu, Japan. *J. Meteor. Soc. Jpn*, **78:** 835–856.

List of Figures

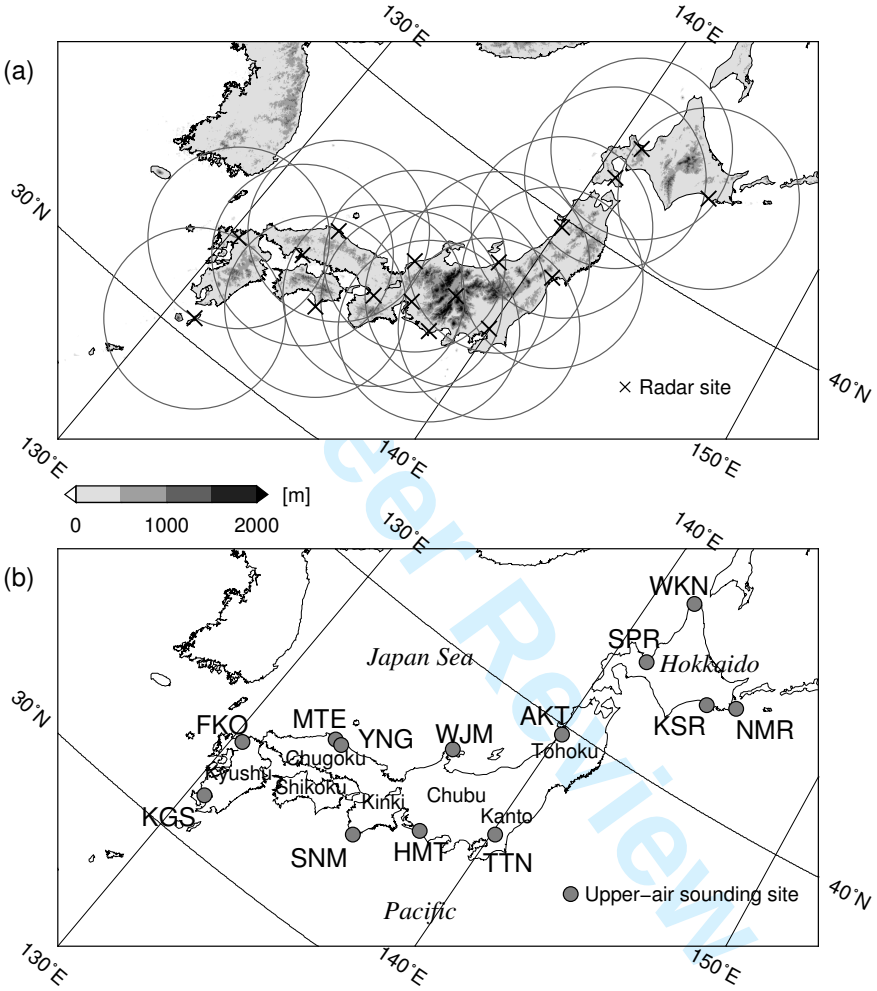

Figure 1. The locations of (a) the operational radar (indicated by crosses) and (b) the radiosonde sites (gray circles). In (a), the detecting ranges of the operational radar are displayed with solid circles, and the shade indicates surface elevation with the 500-m interval. See the texts for the acronyms of the radiosonde sites indicated in (b).

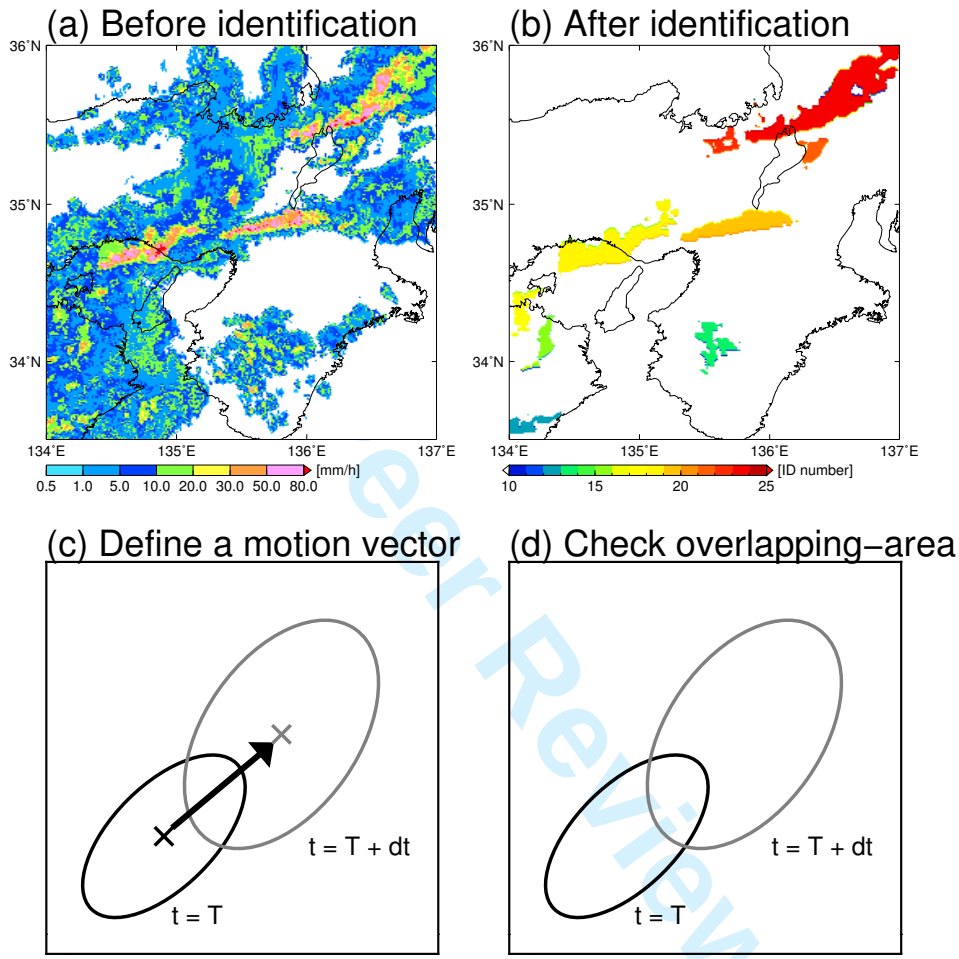

Figure 2. The schematic procedures to extract QSCCs in this study. (a) An original distribution of precipitation intensity (mm h^{-1}) before identifying CCs. The threshold value of 10 mm h^{-1} is for the minimum precipitation intensity to determine a contiguous area of CCs. (b) A result of extracting CCs. Color indicates individual ID numbers for the CCs. (c) The motion vector in the tracking procedure. (d) The case where a part of the CC at t = T and a part of the CC at t = T + dt are overlapped.

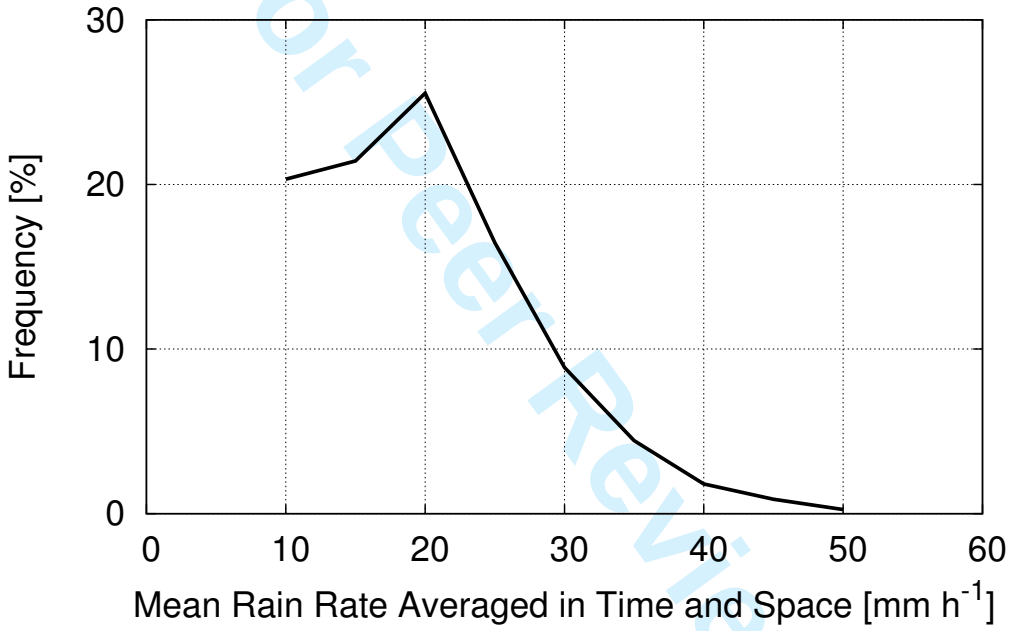

Figure 3. Frequency distribution of the time-mean precipitation intensity averaged for the lifetime of each QSCC, counted at the interval of 5 mm h^{-1}. The frequency at a rain rate r means the value accumulated over the rain rate between r-2.5 and r+2.5.

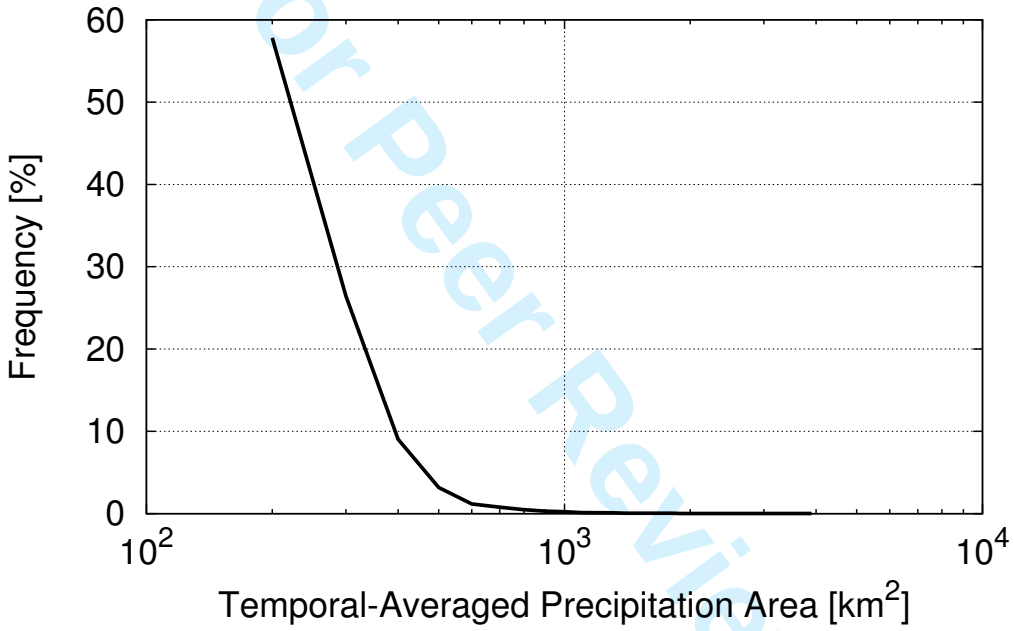

Figure 4. The same as Figure 3, except for the time-averaged precipitation area for the QSCCs, accumulated at the interval of 100 km^2 and the range from a-50 to a+49, where a is a precipitation area.

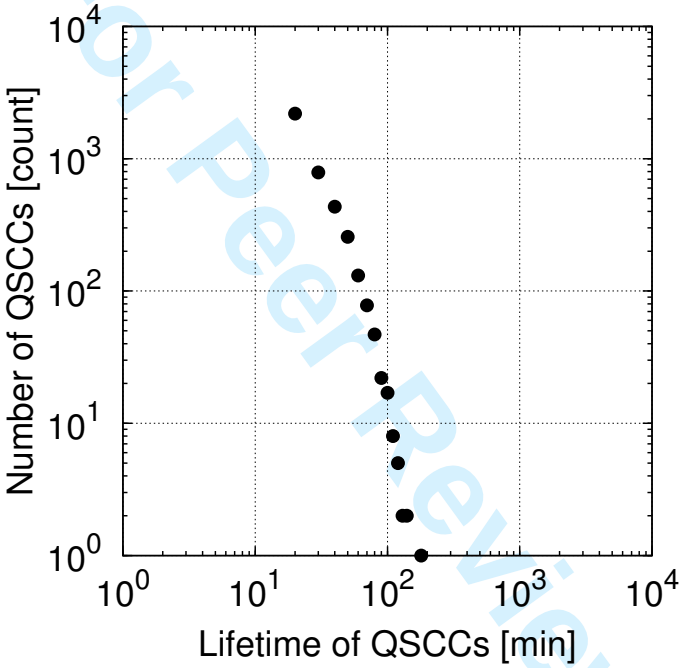

Figure 5. Number of QSCCs with respect to their lifetimes, counted at the 10-minutes interval.

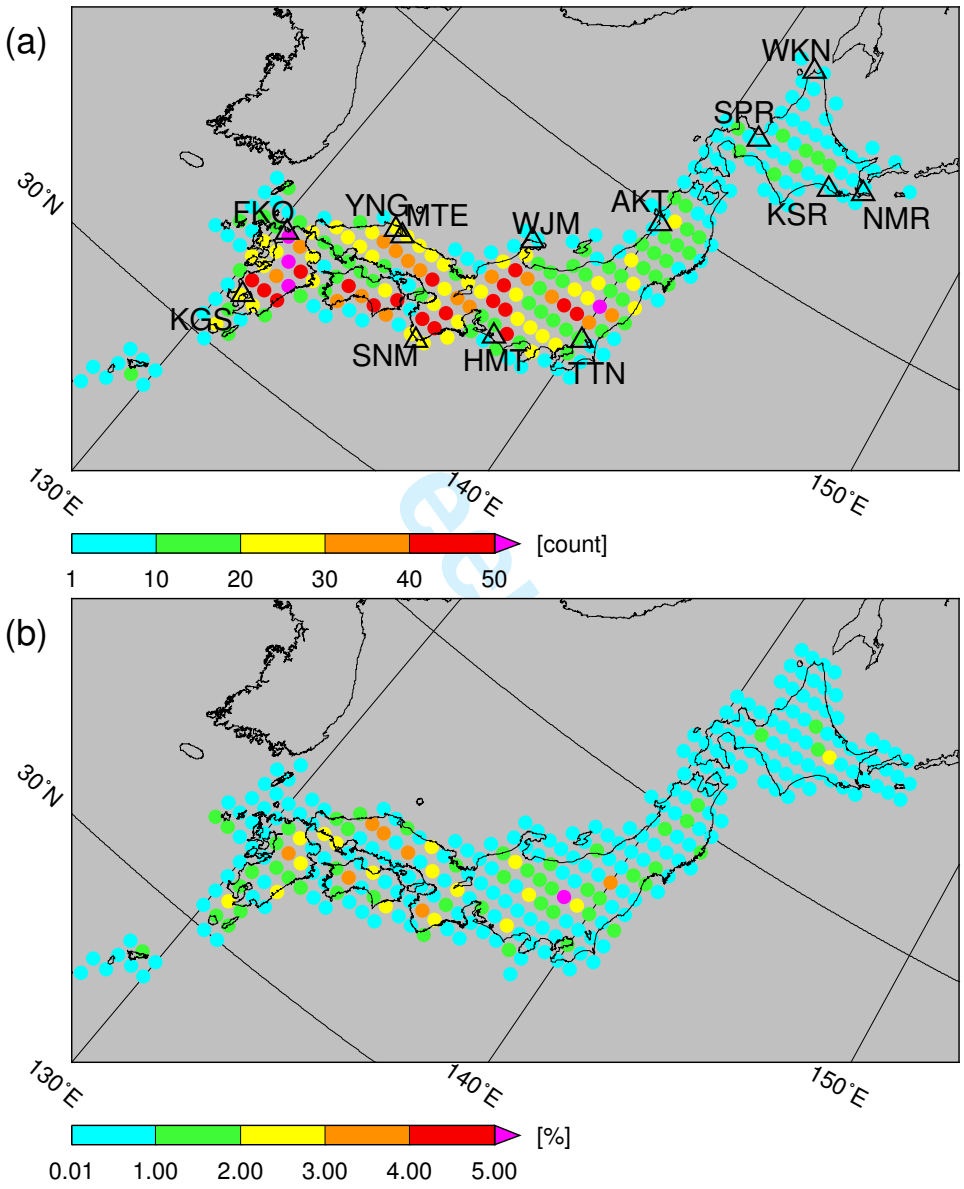

Figure 6. (a) The frequency distribution of QSCCs that evaluated over the 50-km^2 area. (b) The same as (a) but the percentage of the rainfall that is produced by QSCCs to the total rainfall during the warm season. The locations of the radiosonde sites are indicated by triangles at (a).

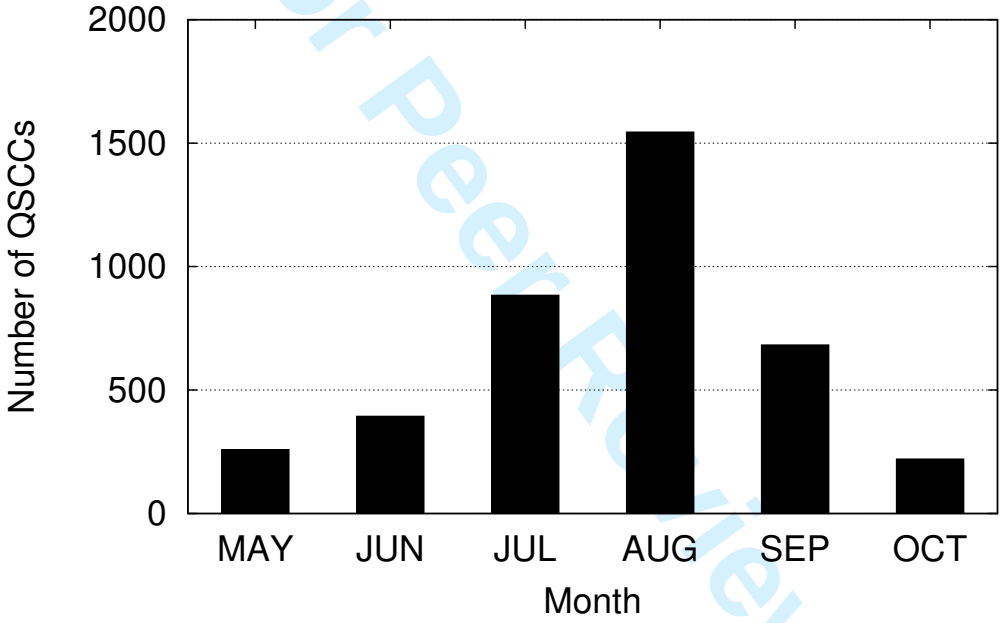

Figure 7. Month-to-month change of the occurrence of QSCCs.

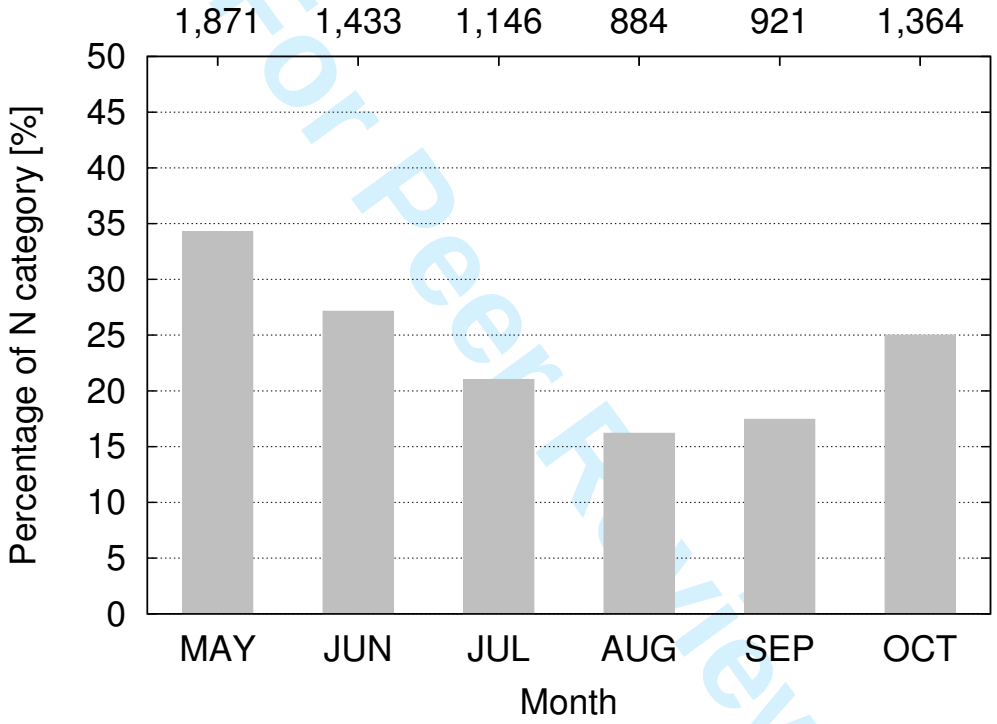

Figure 8. Percentage of the frequency of the no-rain cases (N category) to all the radiosonde observation times. Actual numbers of the N category are given on the upper horizontal axis.

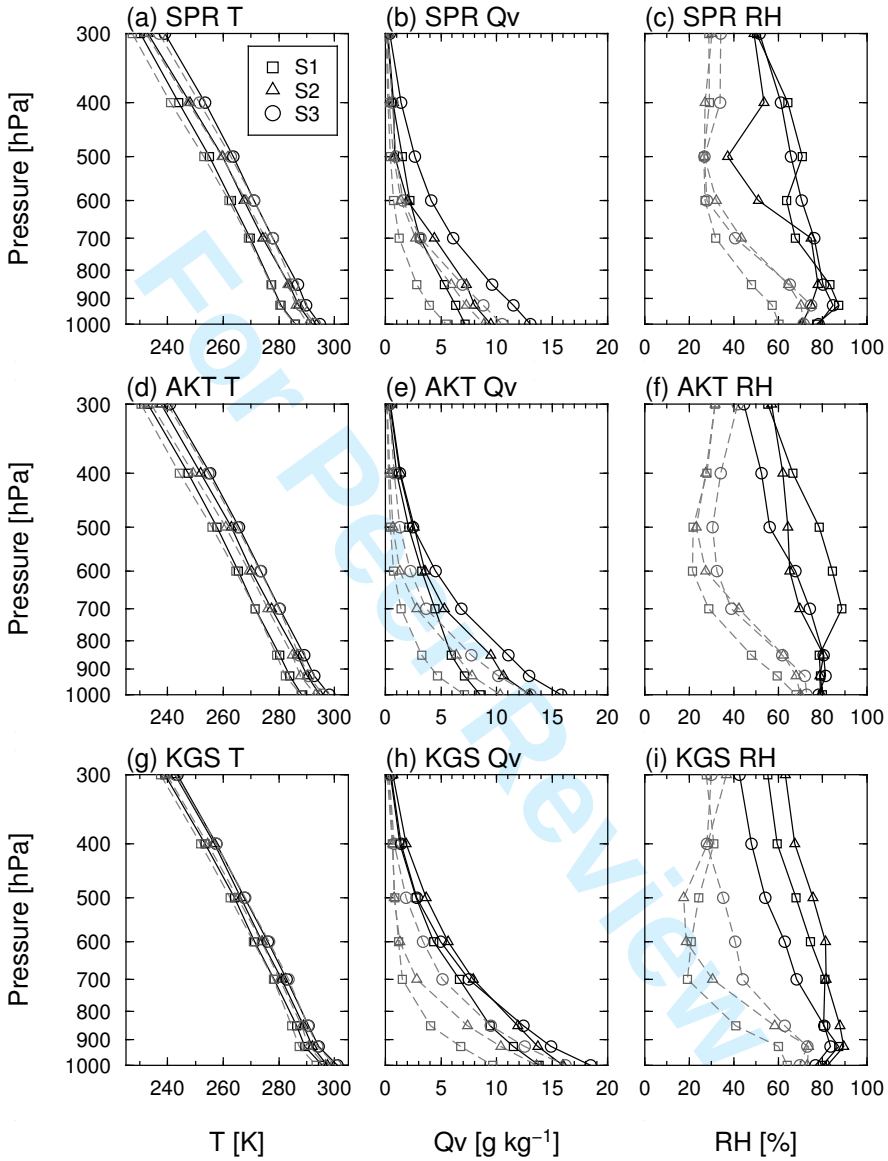

Figure 9. The vertical profile of the mean temperature in (a) SPR, (d) AKT, and (g) KGS, the mean water vapor mixing ratio in (b) SPR, (e) AKT, and (h) KGS, and the relative humidity in (c) SPR, (f) AKT, and (i) KGS averaged from radiosonde observations in each site of QSCCs (Q, black solid line) and no-rain cases (N, gray dashed line). The rectangle, triangle, and circle show the profiles for S1 (May; Octorber), S2 (June), and S3 (July–September), respectively.

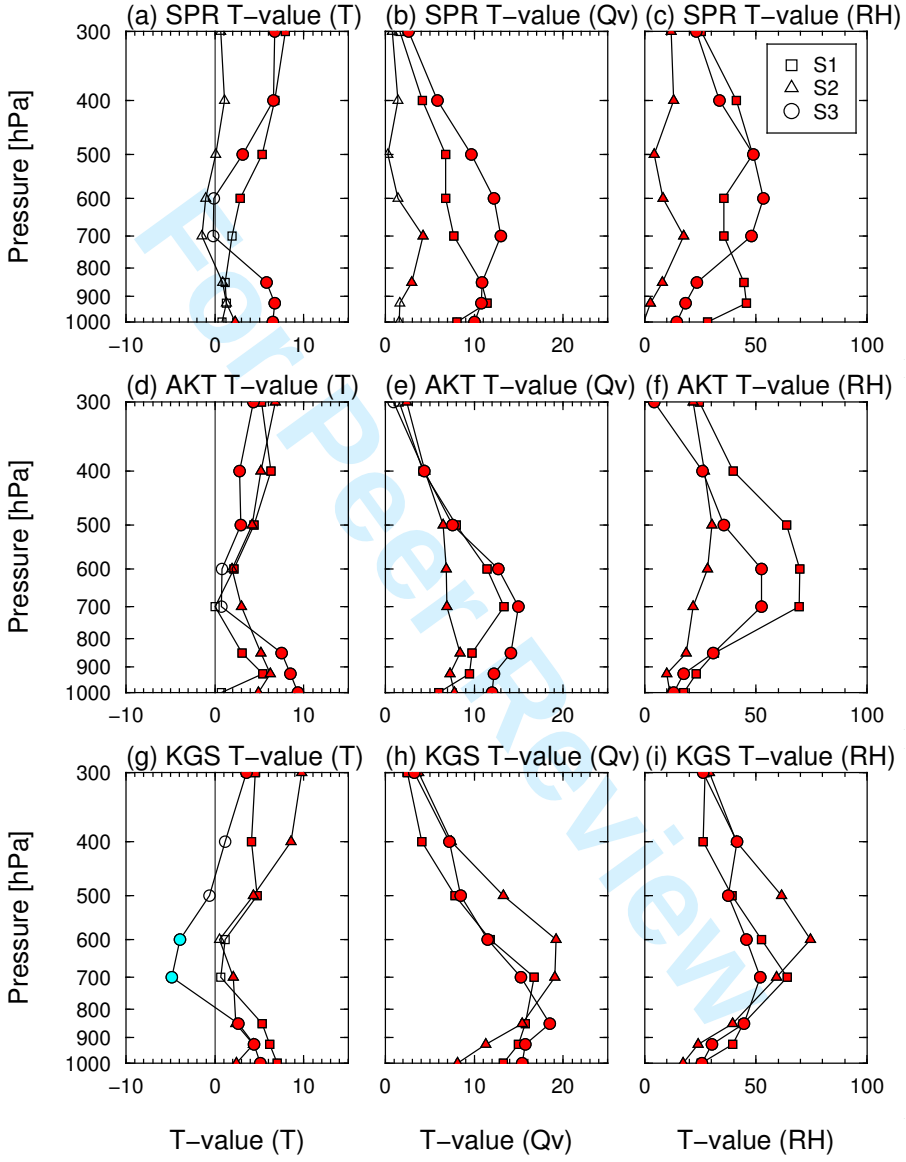

Figure 10. The same as Figure 9, except for the T-values of the differences in the mean values between QSCCs (Q) and no-rain cases (N). The red and cyan marks indicate that the values are significantly different at the 95% confidence level.

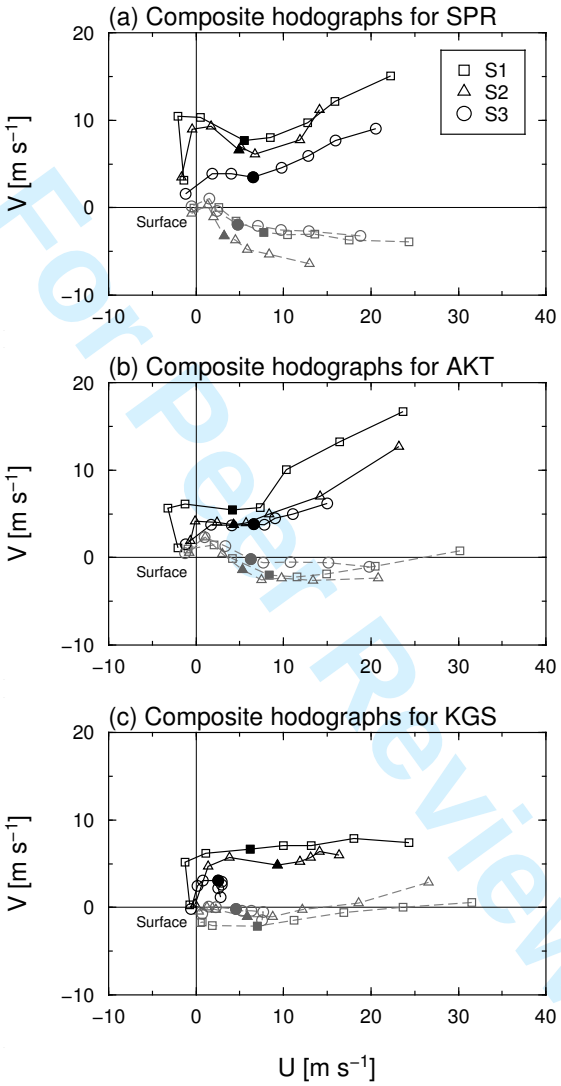

Figure 11. The mean wind hodograph in (a) SPR, (b) AKT, and (c) KGS averaged from radiosonde observations in each site of QSCCs (Q, black solid line) and no-rain cases (N, gray solid line). The rectangle, triangle, and circle indicate the hodographs for S1 (May; Octorber), S2 (June), and S3 (July–September). The filled marks indicate the wind at the 700-hPa level.

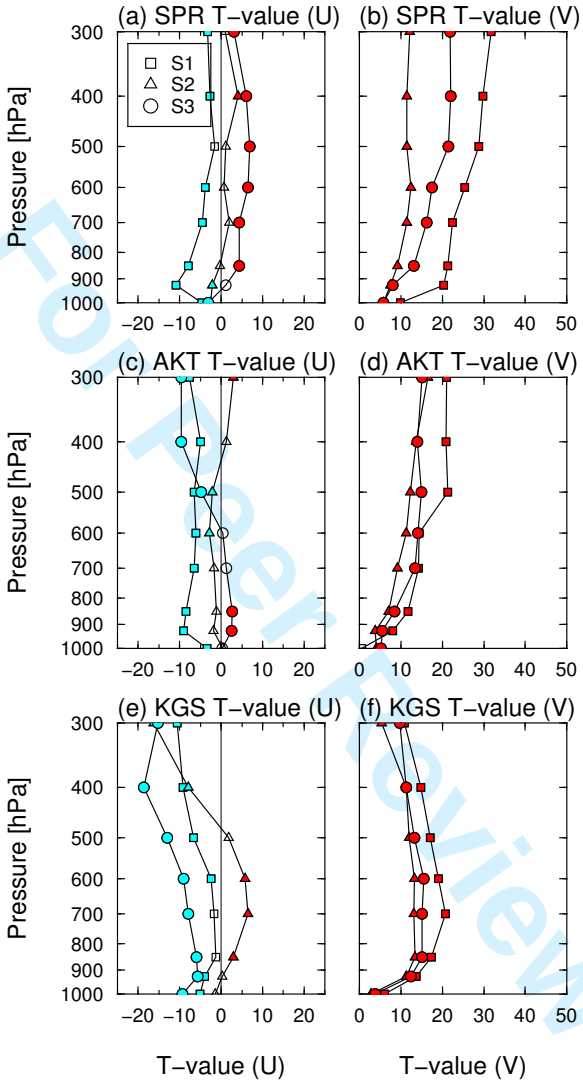

Figure 12. The vertical profile of T-values of the differences in the mean values of (a) (c) (e) the zonal wind speed, and (b) (d) (f) the meridional wind speed between QSCCs (Q) and no-rain cases (N) for (a) (b) SPR, (c) (d) AKT, and (e) (f) KGS. The rectangle, triangle, and circle indicate the hodographs for S1 (May; Octorber), S2 (June), and S3 (July–September). The red and cyan marks indicate that the values are significantly different at the 95% confidence level.

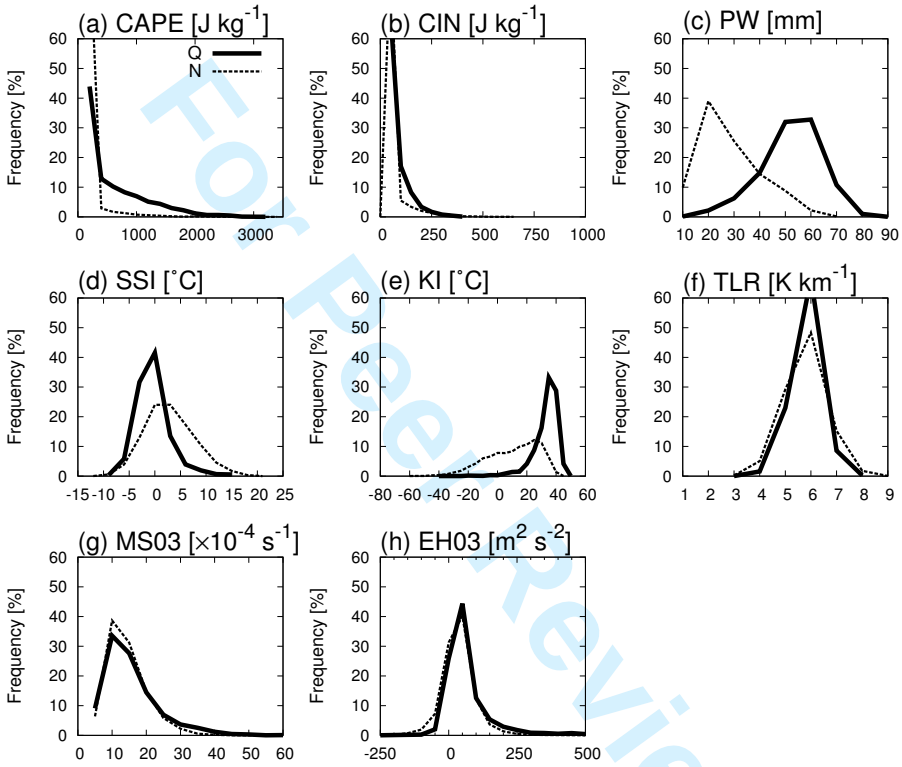

Figure 13. Frequency distributions of the environmental parameters calculated from radiosonde observations for QSCCs (Q) and no-rain cases (N). (a) CAPE [J kg^{-1}], (b) CIN [J kg^{-1}], (c) PW [mm], (d) SSI [°C], (e) KI [°C], (f) TLR [K km^{-1}], (g) MS03 [$\times 10^{-4}$ s^{-1}], and (h) EH03 [m^2 s^{-2}]. Black solid line and gray dashed line indicate the values of Q and N, respectively. The frequency intervals in (a)–(h) are 200, 50, 10, 3, 5, 1, 5, and 50, respectively. The values show the frequencies that are accumulated at the center of the intervals.

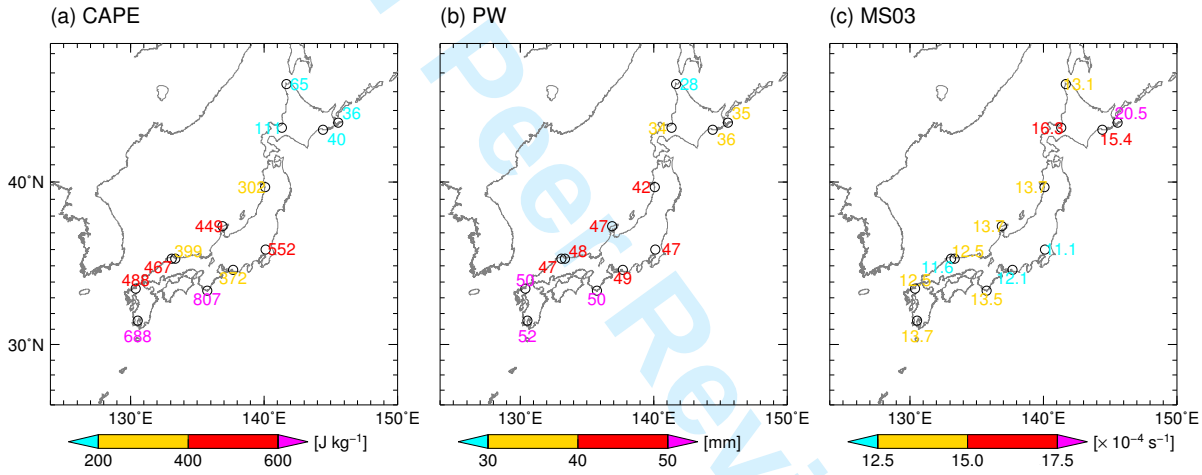

Figure 14. The distributions of the warm-season-mean environmental parameters of (a) CAPE, (b) PW, and (c) MS03 calculated from radiosonde observations for QSCCs.

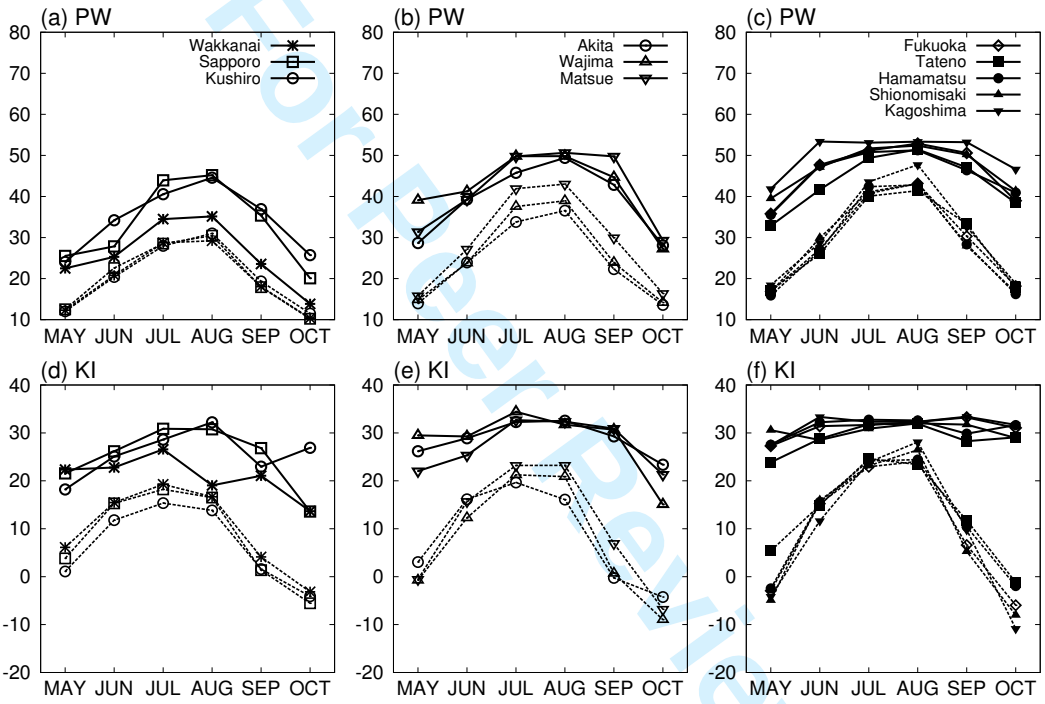

Figure 15. Monthly averages of the regional-mean environmental parameters calculated from radiosonde observations for QSCCs (Q) and no-rain cases (N): PW in (a)–(c); and KI in (d)–(f). Black solid line and gray dashed line indicate Q and N, respectively.

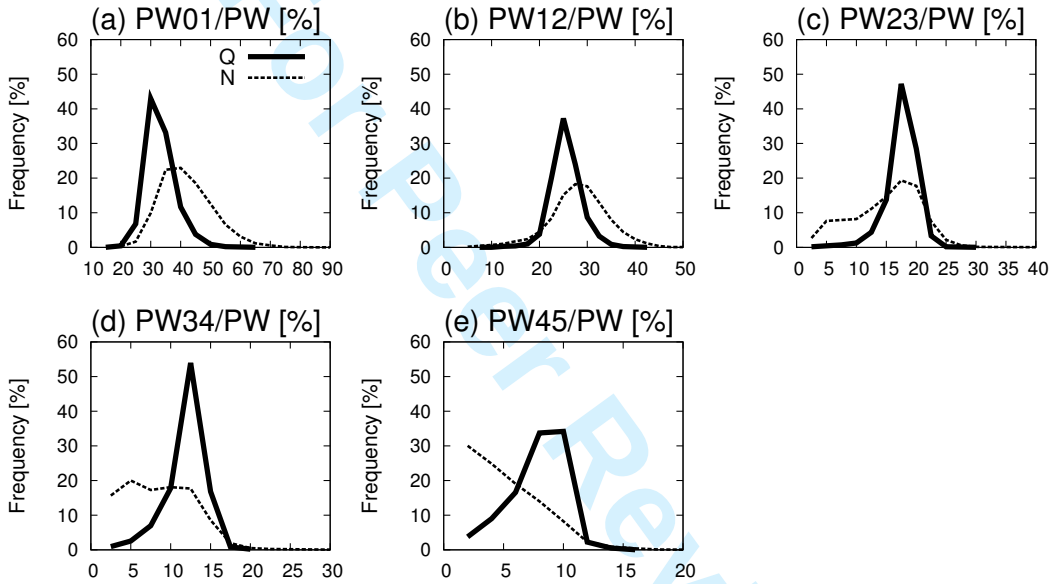

Figure 16. The percentage of the layer-integrated moisture content to the precipitable water in the layer of of (a) 0–1 km, (b) 1–2 km, (c) 2–3 km, (d) 3–4 km, and (e) 4–5 km of radiosonde observations (all 11 sites) for QSCCs (Q, solid line) and no-rain cases (N, dashed line). The frequency intervals in (a), (b)–(d), and (e) are 5, 2.5, and 2, respectively. The values show the frequencies that are accumulated at the center of the intervals.

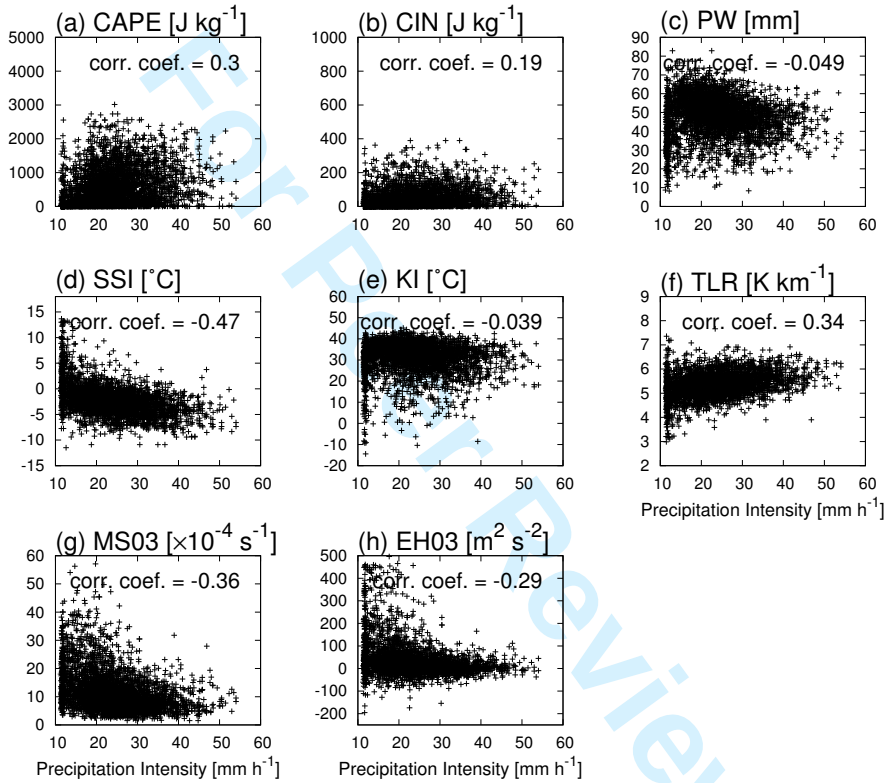

Figure 17. The relationships of the mean precipitation intensity averaged in time and space for the QSCCs with (a) CAPE, (b) CIN, (c) PW, (d) SSI, (e) KI, (f) TLR, (g) MS03, and (h) EH03. Correlation coefficients between the precipitation intensity and the environmental parameters were also given at the upper-right corner in each panel.

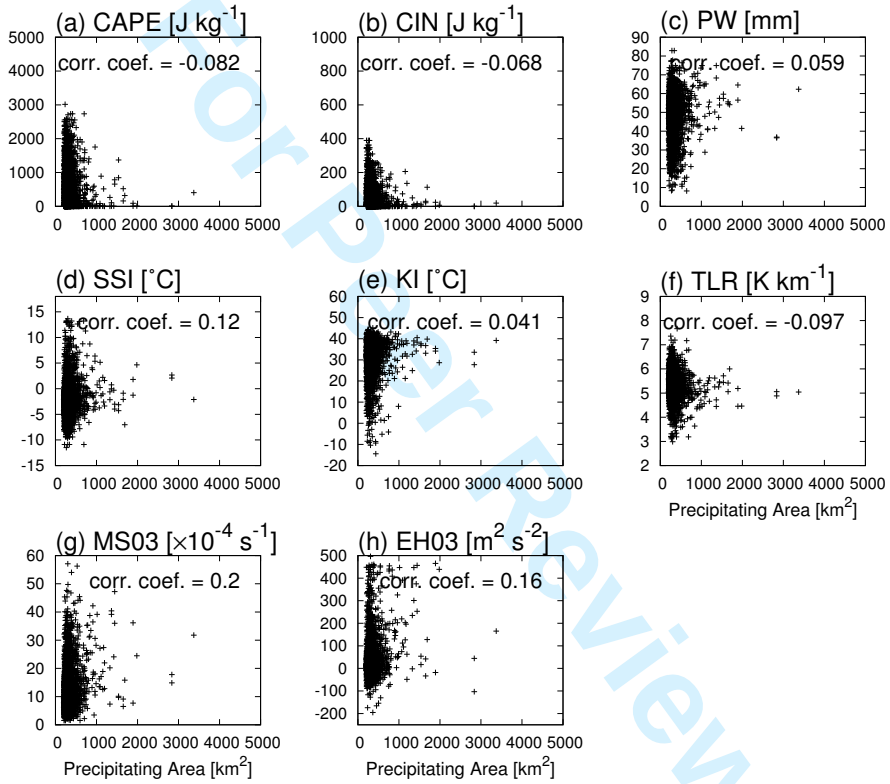

Figure 18. The same as Figure 17, except for the time-averaged precipitation area for the QSCCs.

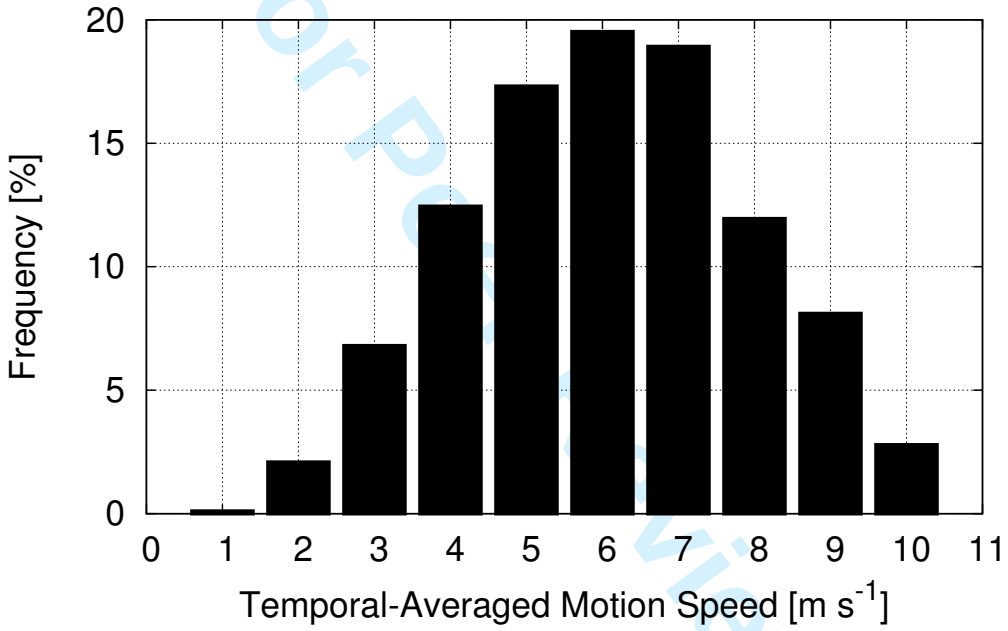

Figure 19. Frequency distribution of the time-averaged motion speed for the convective clusters, accumulated at the interval of 1 m s^{-1} and the range from v-0.5 to v+0.4, where v is a motion speed.

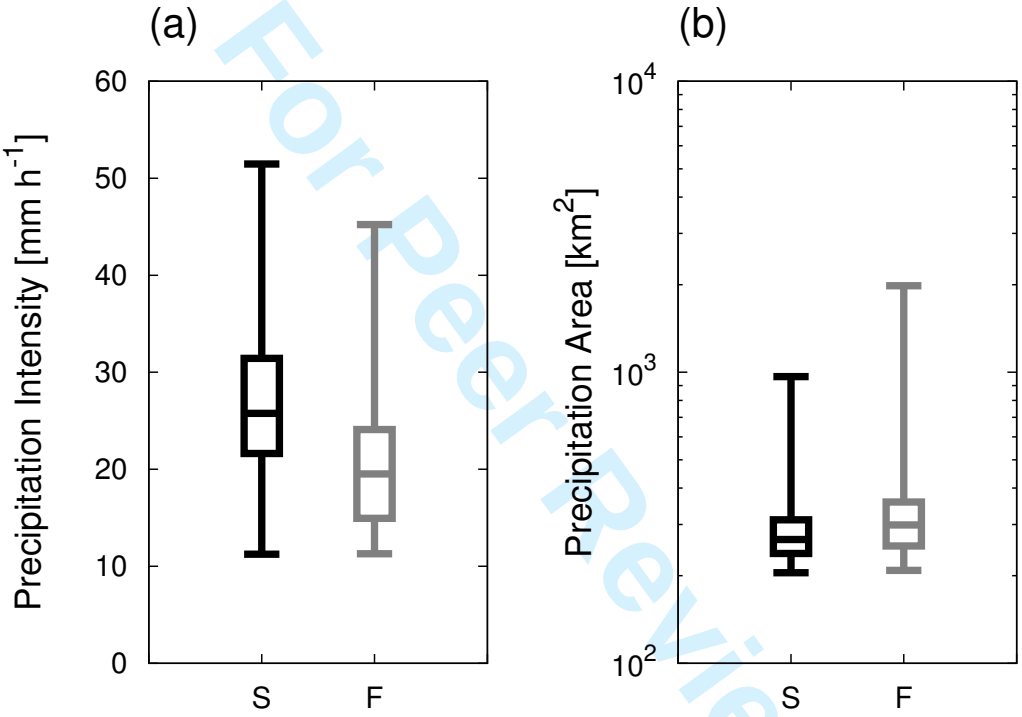

Figure 20. The box-and-whisker plot of (a) precipitation intensity and (b) precipitation area for slow-moving (S) and fast-moving (F) categories. The whiskers at the upper and lower ends indicate the maximum and the minimum, respectively. The top and bottom lines of each box mean the 75 and 25 percentiles, respectively. The middle line in each box shows the median.

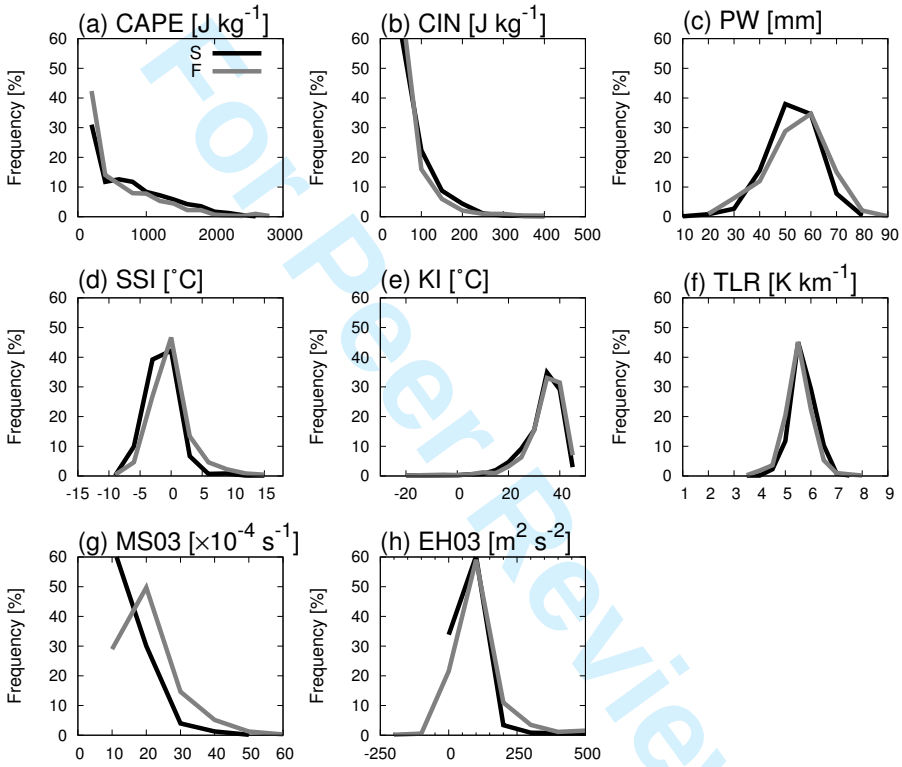

Figure 21. The same as Figure 13, except for slow-moving (S, black) and fast-moving (F, gray) categories. The frequency intervals in (a)–(h) are 200, 50, 10, 3, 5, 1, 5, and 50, respectively. The values show the frequencies that are accumulated at the center of the intervals.

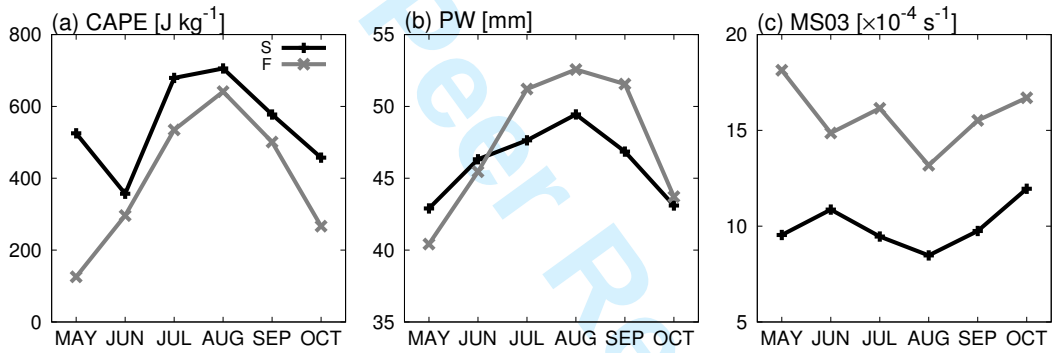

Figure 22. Monthly values of the regional-mean values of (a) CAPE, (b) PW, and (c) MS03 for slow-moving (S, black) and fast-moving (F, gray) categories.

List of Tables

Table 1. The mean, standard deviation, and T-value of the environmental parameters between QSCCs (Q) and no-rain cases (N). Parameters with an asterisk (*) indicate that the mean values between Q and N are significantly different at the 95% confidence level.

Parameters	Average (Standard deviation) Q		N		T-value (Q-N)
CAPE [J kg^{-1}]	489	(554)	69.7	(236)	35.8*
CIN [J kg^{-1}]	44.1	(58.5)	24.5	(63.2)	14.0*
PW [mm]	47.4	(11.5)	23.1	(11.8)	89.3*
SSI [C°]	-1.9	(3.3)	1.4	(4.7)	-37.8*
KI [C°]	30.7	(8.40)	7.98	(17.8)	85.1*
TLR [K km^{-1}]	5.31	(0.524)	5.29	(0.78)	1.28
MS03 [$\times 10^{-4}$ s^{-1}]	13.0	(7.83)	11.8	(6.23)	6.56*
EH03 [m^2 s^{-2}]	47.2	(107)	10.9	(61.7)	15.7*

Table 2. The same as Table 1, except for slow-moving (S) and fast-moving (F).

Parameters	Average (Standard deviation) S		F		T-value (S-F)
CAPE [J kg^{-1}]	625	(564)	486	(550)	4.71*
CIN [J kg^{-1}]	50.4	(56.8)	37.1	(53.5)	4.53*
PW [mm]	47.8	(9.35)	49.4	(11.5)	-2.93*
SSI [C°]	-2.9	(2.6)	-1.6	(3.2)	-8.73*
KI [C°]	30.9	(7.39)	31.8	(7.83)	-2.30*
TLR [K km^{-1}]	5.42	(0.444)	5.25	(0.507)	6.52*
MS03 [$\times 10^{-4}$ s^{-1}]	9.49	(5.73)	15.0	(8.26)	-14.5*
EH03 [m^{-2} s^{-2}]	22.1	(69.7)	61.9	(121)	-7.60*